Study of the Vibrational Spectra and Absorption Cross Sections of 1-chloro-1-fluoroethene by a Joint Experimental and *Ab Initio* Approach

Andrea Pietropolli Charmet,[†,*], Paolo Stoppa,[†] Nicola Tasinato,[‡] Santi Giorgianni,[†] Alberto Gambi[§]

[†] Dipartimento di Scienze Molecolari e Nanosistemi, Università Ca' Foscari Venezia, Via Torino 155, 30172 Mestre (Ve), Italy.

[‡] Scuola Normale Superiore, Piazza dei Cavalieri 7, 56126 Pisa (Pi), Italy.

[§] Dipartimento Politecnico di Ingegneria e Architettura, Università degli Studi di Udine, Via Cotonificio, 108, 33100 Udine (Ud), Italy.

KEYWORDS: Vibrational Analysis; Anharmonic Resonances; Darling-Dennison Resonances; Hybrid Force Fields; Cross Section Spectra.

[*] corresponding author (Tel: +39 041 2348541; Email: jacpnike@unive.it)

ABSTRACT

The gas-phase infrared spectra of 1-chloro-1-fluoroethene (geminal chloro-fluoroethene, $ClFC=CH_2$, 1,1-C_2H_2ClF) were recorded at medium resolution in the range 400 – 6400 cm^{-1} and the vibrational analysis led to revised assignments for the ν_{11} (A" symmetry), ν_2 (A' symmetry) and ν_1 (A' symmetry) bands. Besides the fundamentals, all the most important spectral features were interpreted in terms of overtone and combination bands, thus obtaining an accurate description of the vibrational structure of $ClFC=CH_2$. Accurate measurements of absorption cross section spectra were carried out and integrated band intensity data were determined. High-level *ab initio* calculations of harmonic and anharmonic force fields thoroughly supported and guided the analysis and the disentangling of the several strongly coupled polyads involving many vibrational levels. Diagonalization of the effective Hamiltonian with the off-diagonal elements involving several Fermi and Darling-Dennison resonance coefficients computed by the theoretical cubic and quartic force constants provided the predicted energy levels in good agreement with the vibrational assignments. The calculated infrared intensities, obtained by taking into account anharmonic corrections, were compared to the accurate experimental absorption cross section data here determined.

1. INTRODUCTION

The last decade has seen a renewed interest in halogenated ethenes, which have been the subjects of many experimental and computational studies. Among the halocarbons, their impact as organic pollutants[1-3] with well known severe toxic effects, makes highly desirable the detecting and quantifying of their presence in the environment. Concerning the different available techniques, infrared spectroscopy is one of the most effective for environmental monitoring, provided that data of sufficient accuracy are available.[4] High-resolution spectroscopy is able to yield the requested molecular constants,[5-8] but the rovibrational analysis of the spectra of halocarbons is often complicated due to the congestions of the absorptions coming from low vibrational states and different isotopologues, and the presence of anharmonic and Coriolis interactions. Reliable band assignments combined with accurate modeling of vibrational couplings and high-level *ab initio* calculations provide the detailed basic data that,[9-11] coupled to the different experimental methods developed for reducing the spectral congestion (for example the use of cooling cells,[12-15] and supersonic jet expansion[16-21]) and with the aid by sophisticated data-processing techniques,[22-27] are necessary to guide and support the rovibrational analysis. Besides the spectroscopic interest due to the environmental issues related to the presence of haloethenes in the atmosphere, the potential threat to the stratospheric ozone layer related to their photodissociation and corresponding release of halogen atoms motivated many studies on the elimination mechanisms and distributions of kinetic energy,[28-31] the kinetics of their reactions with $O(^3P)$,[32] and their photochemistry.[33,34]

As short-chain organic compounds, halogenated ethenes are small enough to be accurately modeled by *ab initio* methods and several computational approaches up to high-level state-of-the-art ones. They can be employed as test molecules to compare different approaches and therefore many theoretical works focusing on the prediction of properties like for example stabilities,[35,36] thermochemical data,[37] on their use for benchmarking accurate equilibrium structures,[38,39] and on the performances of different computational methods[40,41] have been recently published for some of

them. Being considered trace gas pollutants, the kinetics of their reactions with $O(^3P)$,[42] and their photochemistry[33,34] and adsorption[43-45] on substrates suitable for subsequent photodegradation have also been investigated. For supporting the monitoring by means of spectroscopic techniques studies dealing with the computation of the vibrational frequencies, the analysis of resonances and determination of anharmonic constants from the assignments of low-resolution infrared spectra have been carried out for some halogenated ethenes. [46-49]

Regarding 1-chloro-1-fluoroethene (geminal chloro-fluoroethene, 1,1-C_2H_2ClF, $ClFC=CH_2$), the microwave data, first measured by Stone and Flygare[50] were later refined in the millimeter wave region by Alonso *et al.*,[51] and then analyzed[52,53] by means of two dimensional Fourier transform spectroscopy. Leung *et al.*[54] some years ago reported on the rotational constants derived from the microwave spectra of eight isotopic modifications thus obtaining both average and Kraitchman substitution structures; subsequent studies on the molecular structure of 1-chloro-1-fluoroethene-hydrogen fluoride complex were described.[55] By using synchrotron radiation, the photoabsorption spectrum between 5 and 15 eV was recently analysed,[56,57] and the valence/Rydberg transition region centered around 7 eV was investigated, thus extending the previous available data.[58] In addition, its adiabatic ionization energy has been recently[59] computed by CBS method and its first two ionic states have been studied by employing both time-dependent and time-independent density functional theories.

Besides, because of its toxicity both its removal in case of accidental release as well as the detection and monitoring of its presence in the atmosphere are highly desirable. Concerning the monitoring, the need of accurate spectroscopic data to support the detection of this molecule by means of infrared techniques motivated the recording of high-resolution infrared spectra and the rovibrational analysis of some important absorptions falling in the region of atmospheric interest.[60,61] For its removal from the atmosphere, the degradation by means of heterogeneous photocatalysis represents a promising approach, and therefore its adsorption on TiO_2 was investigated by analyzing the modifications of its vibrational spectra by using infrared spectroscopy

and quantum-mechanical simulations.[62] Nevertheless, the only available data on the vibrational assignment date back to the low-resolution infrared and Raman investigations reported long time ago.[63-65] In these studies, besides ambiguities in the interpretation of the spectral features derived from the presence of many signals due to impurities, the proposed assignment of the bands was carried out mainly by correlating them with the positions of the fundamentals which, at that time, were assigned for CH_2=CF_2 and CH_2=CCl_2. It is worthwhile to note that for 1,1-difluoroethene assignments, especially the origins of both the anti-symmetric and symmetric CH_2 stretchings, were revised and later definitely reassigned.[47]

In the present work, to support further high-resolution studies as well as to improve the modeling of its adsorption on different substrates, we present a detailed study of the vibrational spectra of this molecule coupled with an accurate determination of the corresponding integrated intensities. The spectral region from 400 to 6400 cm^{-1} was investigated and all the most important spectral features were assigned in terms of fundamental, overtone and combination bands, and their intensities were accurately retrieved. High-quality *ab initio* calculations, carried out by employing different levels of theory and basis sets, supported the vibrational analysis by the derivation of potential energy surfaces up to the fourth-order force constants in the space of normal coordinates. To be more precise, reliable harmonic frequencies and their corresponding anharmonic corrections were computed at the coupled cluster level of theory with single and double excitations augmented by a perturbational estimate of the effects of connected triple excitations,[66-68] CCSD(T), as well as at MP2[69] and double hybrid B2PLYP[70,71] level of theory: concerning the intensities, the corrections to the harmonic values calculated at CCSD(T) level of theory were yielded by terms calculated at MP2 and B2PLYP level. The high density of vibrational transitions (especially in the region of CH_2 stretchings) led to several anharmonic resonances (Fermi and Darling-Dennison), whose effects in the corresponding polyads of different vibrational states must be taken into account. In order to better understand their relative importance, also the criteria recently proposed by Krasnoshchekov *et al.*[72] were used. As it will be explained in the next section, the choice of the basis set was

mandatory for a comprehensive assignment of the infrared spectrum and going into details it avoids the mislabeling of the resonant couple $\nu_3/2\nu_{10}$.

2. EXPERIMENTAL AND COMPUTATIONAL DETAILS

We carried out the vibrational analysis on the gas-phase absorption spectra of 1-chloro-1-fluoroethene recorded at room temperature in the range 400 – 6400 cm^{-1}. The spectra were recorded at medium resolution (from 1.0 cm^{-1} up to 0.2 cm^{-1}) by using a Bruker Vertex 70 FTIR instrument and employing a double walled, stainless steel cell, fitted with KBr windows and with an optical path-length of 134.0 (±0.5) mm. To improve the signal-to-noise ratio (SNR), 128 scans were acquired, and the pressure of the sample was varied in the range 0.1–660 hPa. For obtaining absorption cross section the temperature within the cell was kept constant at 298.0 K (±0.5 K) and the SNR was maximized by adding up to 256 interferograms. Taking into account the effects of finite resolution[73,74] and the corresponding instrumental distortion, we adopted the experimental procedure already established in previous studies[75] by mixing the sample with N_2 (purchased by SIAD, Italy, with a purity >99%) to a total pressure of 101 kPa. By using a diffusion pump backed by a double stage rotary pump the cell was evacuated to about 10^{-4} Pa before and after the recording of every measurement, and the corresponding background spectra were recorded. Concerning the adsorption of the gas sample on the cell walls, we monitored it both by directly measuring the pressure, and by checking the absorption spectrum;[76] it was found not significant over longer period than that used to record a spectrum. The commercial sample of 1-chloro-1-fluoroethene was supplied by LANCASTER (stated purity > 97%) and we used it without any further purification.

Concerning the quantum chemical calculations carried out at CCSD(T) level of theory, at first, we optimized the molecular geometry and computed the harmonic force field at the

corresponding equilibrium structure. The anharmonic force fields, computed in subsequent runs, expressed in terms of cubic and quartic semi-diagonal force constants were evaluated in the normal coordinates space by numerical differentiation of the analytic second derivatives calculated at points displaced along the normal coordinates,[77] using a step size ΔQ = 0.05 amu$^{1/2}$ bohr. Different correlation consistent Dunning basis sets were employed in order to get the best frequency evaluation and they will be discussed here (another group of basis sets were used to obtain the best geometry and will be reported in a next work).[78] The correlation consistent polarized valence triple zeta cc-pVTZ basis,[79-81] which is a [5s, 4p, 2d, 1f / 4s, 3p, 2d, 1f / 3s, 2p, 1d] contraction of a (15s, 9p, 2d, 1f / 10s, 5p, 2d, 1f / 5s, 2p, 1d) primitive set for Cl / C, F / H atoms, respectively, was used in the frozen core (fc) approximation (this basis set is hereafter labeled as VTZ). With this basis set, a cubic (complete) and quartic (semi-diagonal force constants) anharmonic force field was determined. In order to improve the overall assignment of frequencies which gave errors too large compared to the experimental values, the augmented cc-pVTZ basis set[79,80] (11s, 6p, 3d, 2f) / [5s, 4p, 3d, 2f] was employed for the fluorine atom to derive the corresponding geometry and harmonic frequencies. This basis set, referred to as VTZ-AVTZ(F) in the present work, avoids the known problems (low accuracy)[82] related to the use of diffuse function to the triple-ζ basis for all the atoms in haloethenes. With this run, also carried out in the frozen core approximation, the harmonic force field, determined at the optimized geometry, was used in conjunction with the anharmonic force constants computed with the VTZ basis set. Employing this hybrid force field, a general improvement of the data calculated was observed, however, not yet sufficient for some bands and in particular for the resonant couple $\nu_3/2\nu_{10}$. Using the correlation consistent polarized core/valence triple zeta basis set cc-pCVTZ[79,83,84] for Cl, C whereas the aug-cc-pCVTZ[80,84] basis set was employed for the F atom (in the present work this basis set is referred as CVTZ-ACVTZ(F)), the harmonic force field was evaluated (all the electrons were correlated) and used in conjunction with the anharmonic terms previously computed with the VTZ basis set. Since the improvement

achieved by this hybrid computation was not considered satisfactory to resolve the resonant dyad $\nu_3/2\nu_{10}$, also the anharmonic force field was evaluated employing the CVTZ-ACVTZ(F) basis set (all electrons correlated). There was a general improvement in the overall assignment: the computed data led to assign all the most important features unambiguously and without any mislabeling of the bands when treating the Fermi resonance affecting the vibrational states $v_3 = 1$ and $v_{10} = 2$. We performed a further calculation employing the atomic natural orbital sets introduced by Taylor and Amlöf[85] with [5s, 4p, 3d, 2f, 1g / 4s, 3p, 2d, 1f] contractions for C, F / H atoms and [6s, 5p, 3d, 2f] for the Cl atom (ANO2 basis set).[86] Core correlation effects were excluded from the calculations and all cubic and semi-diagonal quartic constants were calculated by numerical differentiation of analytic second derivatives, at the optimized geometry, as discussed earlier. We carried out all these calculations with the CFOUR suite of programs.[87]

Besides these calculations carried out at CCSD(T) level of theory, we performed additional computations at lower level employing the Gaussian09 software:[88] namely, MP2 (within the frozen core approximation) and B2PLYP level of electronic correlation were employed in conjunction with the CVTZ-ACVTZ(F) basis set previously described to compute the derivatives of the potential energy surface (PES) up to cubic and quartic semi-diagonal terms.

We employed the cubic and quartic semi-diagonal force constants calculated for computing anharmonic corrections to the harmonic wavenumbers in the framework of vibrational second-order perturbation theory, VPT2.[89-91] This theory has the advantage of the avaibility of analytic formulas for obtaining several spectroscopic parameters (ro-vibrational constants, α, anharmonic constants, $x_{i,j}$, etc.). These expressions, however, may suffer from singularities, and therefore lead to large errors in the corresponding computed quantities, in case of first order resonances called Fermi resonances (FR). These interactions affect two close energy levels differing by three units in their vibrational quantum number (for this reason they are also named vibrational 1-2 resonances); more specifically, they are classified as type I when the difference is equal to one in one mode and two quanta in the other, while they belong to type II when the difference is equal to one in one mode

and two in two different modes. The commonly adopted approach for their proper treatment is performed in a two-step procedure: first, the formulas for computing spectroscopic parameters are converted into expressions with terms which, in the denominators, have linear combination of the harmonic frequencies (ω_i, ω_j, …). Following the criteria proposed by Martin *et al.*,[92] Fermi resonances are then identified by considering frequency differences and evaluating the results coming from a model variational calculation with respect to those obtained by perturbative accounting for the cubic terms. The terms whose denominators are potentially vanishing (flagged as "resonant" terms) and thus leading to near-singularities, are therefore removed from the corresponding equations employed to compute anharmonicity constants, $x_{i,j}$, thus leading to modified ("deperturbed") constants $x^*_{i,j}$ which are now considered unaffected by error due to resonances. Then, the numerical diagonalization of quasi-diagonal Hamiltonian matrices containing the energies of the vibrational levels (which are now computed employing $x^*_{i,j}$ and therefore "deperturbed") and having the corresponding Fermi interactions taken into account by their respective coupling terms, W, yields the final energies. Besides Fermi resonances, there are also couplings which manifest themselves in the second order, called Darling-Dennison resonances (DDR);[93] in addition to the classical 2-2 resonance (when there is the annihilation of two vibrational quanta in one mode and the corresponding creation of two quanta in another), they can have also the form 2-11 (annihilation of two vibrational quanta in one mode and the creation of one quantum in two distinct modes), 11-11 (annihilation of two vibrational quanta in two distinct modes and the creation of two quanta in other two), 1-3 (annihilation of one vibrational quantum in one mode and the creation of three quanta in another), 1-21 (annihilation of one vibrational quantum in one mode and the creation of two quanta in one mode and of one quantum in another), 1-111 (annihilation of one vibrational quantum in one mode and the creation of one quantum in three distinct ones), and 1-1 (with a total change of two vibrational quanta in two different modes).[72] In the presence of DDR the corresponding terms, K_{DD}, are also present in the coupling matrix. Following the classification

recently reviewed by Piccardo *et al.*,[94] we label GVPT2 (Generalized Vibrational second-order Perturbation Theory) this approach for dealing with resonances (both of first order, FR, and second order, DDR) within the framework of VPT2. The presence of Fermi resonances leads to an additional problem for the calculation of the couplings arising from DDR. Within the framework of VPT2 there are analytic expressions for every Darling-Dennison coupling constants (K_{DD}): these equations contain different contributions coming from the quartic force field, the vibrational angular momentum (expressed as combinations of Coriolis zeta constants, $\zeta_{i,j}^{\alpha}$, and harmonic frequencies, ω_i), and from the cubic part of the anharmonic potential. The latter terms have the same kind of resonance denominators as those of the anharmonicity constants, which may therefore lead to singularities when FR occurs. These terms, affected by first order couplings as recognized in literature,[95] should be removed in order to get the corrected results. So, we implemented the second order Darling-Dennison resonances and associated K_{DD} constants[95,96] in a local version of the program SPECTRO:[97] following Martin *et al.*[95] the resonances constants, K_{DD}, are expressed in terms of the *D*-notation:

$$D(\pm k,\pm l,\pm m) = \frac{1}{(\pm\omega_k,\pm\omega_l,\pm\omega_m)} \quad (1)$$

This notation, besides the easy translation into the program code, facilitates treating the effects of resonances because the denominators which are affected by recognized Fermi resonances can be excluded from the summation formula which computes the K_{DD} constants.[95,96,98,99] In the present work the relative magnitude of the several Darling-Dennison resonances thus computed, deperturbed from the effects related to FR, was discussed and compared with respect to the recently suggested criteria for assessing their estimated effects.[72]

In addition, for calculating the anharmonic corrections to the harmonic frequencies computed at higher level, i.e. CCSD(T), we also employed the recently developed hybrid

degeneracy-corrected second-order perturbation theory, HDCPT2,[100] which is a modification of the degeneracy corrected PT2 (DCPT2) approach originally proposed by Kuhler *et al.*[101] for evaluating vibrational energy levels in the presence of resonances.

To compute the anharmonic corrections to the infrared intensities, we used the derivatives of the potential energy surface (PES) and of the dipole moments, carried out at MP2 and B2PLYP level of electronic correlation. Following the procedure established in the precedent studies,[82,102] these terms were employed in conjunction with the harmonic data derived by CCSD(T) calculations to compute two hybrid force fields, labeled HYB-MP2-1 and HYB-B2PLYP-1, having the anharmonic corrections yielded at fc-MP2/CVTZ-ACVTZ(F) and B2PLYP/CVTZ-ACVTZ(F) level of theory, respectively. In addition, other two hybrid force fields were derived (labeled HYB-MP2-2 and HYB-B2PLYP-2) by combining the harmonic part calculated at fc-CCSD(T)/ANO2 level with the anharmonic ones computed at fc-MP2/CVTZ-ACVTZ(F) and B2PLYP/CVTZ-ACVTZ(F), respectively: they have been used to benchmark their anharmonic predictions of intensities with respect to those calculated by correcting the harmonic data obtained at CCSD(T)/CVTZ-ACVTZ(F) level of theory. We used the corrections to harmonic intensities thus obtained for comparing the predicted values to the accurate values of absorption cross sections determined in the present work.

3. RESULTS AND ANALYSIS

3.1. Equilibrium Geometry and Harmonic Force Field Calculation.

The equilibrium structure of 1-chloro-1-fluoroethene was determined at the different levels of theory previously described. Figure 1 reports the $ClFC=CH_2$ molecule with the three principal axes of inertia. In Table 1 are reported the equilibrium geometries obtained at CCSD(T) level of theory employing the basis sets described in the previous section. The correspondence with the chemical intuitive internal coordinates, assuming that the molecule is planar, is also indicated. The

equilibrium rotational constants, being inversely proportional to the moments of inertia (which are derived from the optimized geometry), are related to the molecular structure. Table 1 lists therefore also their values obtained at the corresponding optimized geometries. The harmonic wavenumbers for each of the normal modes (ω_i, i = 1, …, 12) computed with the quadratic force constants at the CCSD(T) level of theory are summarized in Table 2 together with the intensities (km mol^{-1}) computed within the double harmonic approximation. As it can be seen, the major difference concerns the ω_5 value which can be described as a C–F stretching mode: this is a known problem for polar bonds, in particular those involving fluorine atoms, to give a serious overestimation of the C-F stretching frequency.[103,104] The use of aug-cc-pCVTZ basis set on the fluorine atom leads to a consistent improvement in the computed vibrational frequencies which will be much close to the final anharmonic values. By using the quadratic force constants obtained at CCSD(T) level of theory we computed the total energy distribution (TED) with respect to the symmetry adapted internal coordinates. These coordinates were chosen to pinpoint the CH_2 group vibrational modes (stretchings and bendings) and are reported in Table 3. In this Table, r_{ij} represents the bond length between the atoms i and j, α_{ijk} is the angle enclosed by the bonds r_{ij} and r_{jk} with j being the apex atom, τ_{ijkl} is the torsion angle between the planes formed by the atoms ijk and jkl, and γ_{ijkl} is the out-of-plane angle between the bond r_{ij} and the plane defined by the atoms kjl (the atoms are numbered as illustrated in Figure 1). The approximate descriptions of the fundamental vibrations, based on the percentage of TED,[105] are indicated in Table 4. Almost all the vibrational modes are well described by the symmetry coordinates except the ω_5 and ω_6 which show a strong mixing between the C–F stretching and the CH_2 rocking mode.

3.2. Vibrational Assignment of the Gas-Phase Infrared Spectra, and Analysis of Resonances.

We started the vibrational analysis from the spectra recorded at lower pressure to firstly identify all the fundamentals falling in the range 400 – 3200 cm^{-1} (a survey spectrum is depicted in Figure 2). As previously mentioned, the original assignments, proposed by Torkington *et al.*,[63] some years later were revised and extended to all the fundamentals by Mann *et al.*;[64] besides some ambiguities and difficulties in the identification of the spectral features due to the presence of signals related to the impurities in the sample, their assignments were carried out on the basis of the analogous data available at that time for $CH_2=CCl_2$ and $CH_2=CF_2$. Especially in the case of 1,1-difluoroethene, the assignments were later revised and the positions of both the CH_2 stretchings shifted to higher wavenumbers.[47] Therefore we proceeded to verify the positions of all the fundamentals falling in the range investigated taking into account the results of the *ab initio* calculations and the predicted intensities (both harmonic and anharmonic values) and then to assign all the most important remaining absorptions in terms of combination, overtone and hot bands, up to 6400 cm^{-1}. First, we checked the quality of the different anharmonic calculations by comparing their band center predicted values with respect to the experimental ones for all the fundamentals but those related to CH_2 stretchings, since these assignment could be not reliable. Among all the fundamentals, the ν_3 band is significantly perturbed by $2\nu_{10}$ (Fermi type I resonance) and therefore we employed mainly this dyad as benchmark for the different anharmonic calculations previously described: we found that only the ones computed using the CVTZ-ACVTZ(F) basis set and having the harmonic part at CCSD(T)/CVTZ-ACVTZ(F) level were able to correctly treat this interaction and to predict the positions of both ν_3 and $2\nu_{10}$ (observed at 1655.8 cm^{-1} and 1689.6 cm^{-1}, respectively). Among these computations, we decided to employ the one having all the force constants computed at CCSD(T) level of theory for the band center predictions and to use it in conjunction with the data about anharmonic intensities yielded by the others hybrid force fields for supporting the overall spectral assignments. Concerning the fundamentals, the discrepancies between the present assignments and the ones reported in literature are related to the ν_{11}, ν_2 and ν_1

fundamentals. In the following discussion of the vibrational analysis, we therefore first refer to these fundamentals and then present the remaining assignments of the other bands up to 6400 cm^{-1}, grouped according to their positions in the overall spectral region investigated.

3.2.1. The ν_{11} fundamental. This band of A" symmetry, as evident from the TED analysis (see Table 4), involves mainly the torsion of F-C=C-H_4 group; concerning the predictions obtained by the different *ab initio* methods carried out in the present work, its harmonic intensity lie in the range 0.24 – 0.06 km mol^{-1}, while its positions, at the harmonic level, falls in the range 724 – 722 cm^{-1} (see Table 2). Torkington *et al.*[63] reported a weak C-type band around 621 cm^{-1}. Later, Mann *et al.*[64] located this fundamental at 607 cm^{-1}, even if they admitted the presence of spurious signals due to impurities; on the basis of the spectra they presented, the intensity of the signal they attributed to ν_{11} can be estimated to be 5 – 10% with respect to the stronger ν_{12} fundamental (which they centered at 515 cm^{-1}, in good agreement with our value of 514.7 cm^{-1}). Nielsen and Albright however, in their subsequent analysis of Raman spectra,[65] were able to measure all the signals in the regions reported by Mann but the one for ν_{11}. The predicted harmonic intensity for ν_{12} band is 0.78 km mol^{-1} (at CCSD(T)/CVTZ-ACVTZ(F) level of theory), and the predicted anharmonic value lies between 1.08 and 0.73 km mol^{-1}, depending on the hybrid force field, in agreement with the experimentally measured value (0.94 km mol^{-1}, see later); on the basis of the relative intensity of ν_{11} with respect to ν_{12} estimated from the spectra presented by Mann, the ν_{11} should therefore have an intensity falling in the range 0.05 – 0.09 km mol^{-1}. We investigated the region around 610 cm^{-1} by recording different spectra employing sample pressure up to 660 hPa, but we did not observe any signal which can be clearly distinguished from the baseline noise (see Figure 3, which presents the signals recorded in the spectral region 460 – 760 cm^{-1} employing different sample pressures). Moving to the anharmonic computations (see later in the text), the predictions locate this band around 708 cm^{-1} with an intensity which, having a negligible anharmonic correction, is similar to that calculated at harmonic level. On these bases, we therefore revised the original position of this

band shifting it to around 709 cm^{-1} (according to the *ab initio* data) and thus resulting completely covered by the stronger absorption related to the ν_7 fundamental at 700.3 cm^{-1}.

3.2.2 Assignment of the ν_1 and ν_2 fundamentals. These two bands, mainly related to the anti-symmetric (ν_1) and symmetric (ν_2) CH_2 stretchings, were first located by Torkington *et al.*[63] around 3140 cm^{-1} and 3055 cm^{-1}, respectively. Subsequently Mann *et al.*,[65] on the basis of the assignments available at their time for the CH_2 stretchings of 1,1-difluoroethene and 1,1-dichloroethene, suggested the positions centered at 3069 and 3016 cm^{-1} for ν_1 and ν_2, respectively. Concerning 1,1-difluoroethene, the CH_2 stretching bands were definitely located at 3175.6 cm^{-1} (ν_7, anti-symmetric) and 3057.8 cm^{-1} (ν_1, symmetric) by McKean *et al.*,[47] thus revising the value of 3103 cm^{-1} previously accepted for the anti-symmetric CH_2 stretching;[106] subsequently these values were found in agreement with the predictions yielded by high-level theoretical computations.[40] All our harmonic calculations carried out at CCSD(T) level of theory yielded values around 3300 and 3200 cm^{-1} for the anti-symmetric (ν_1) and symmetric (ν_2) CH_2 stretchings, respectively (see Table 2). Concerning the intensities, the ν_1 band computed harmonic value is significantly lower than that of ν_2 (0.23 vs. 3.11 km mol^{-1}, respectively, at CCSD(T)/CVTZ-ACVTZ(F) level of theory): the corrections yielded by all the anharmonic force field data (HYB-MP2-1, HYB-B2PLYP-1, HYB-MP2-2 and HYB-B2PLYP-2) still predict a greater intensity of ν_2 than ν_1. The position of the latter is computed around 3160 cm^{-1} by the different anharmonic force field calculations carried out, while the former, perturbed by different anharmonic resonances which will be discussed in detail later, is expected around 3080 – 3070 cm^{-1}. On these bases, the band located at 3158.9 cm^{-1} in our spectra is assigned as ν_1, while the absorption centered at 3072.1 cm^{-1} is attributed to ν_2 (see Figure 4), thus in line with the assignment originally proposed.[63]

3.2.3. Assignments in the 400 – 600 cm^{-1}. In this spectral region the most important absorptions are due to the ν_8 (A' symmetry) and ν_{12} (A" symmetry) fundamentals. The ν_8 band is located at 432.2 cm^{-1}, in good agreement with its predicted value, which lie in the range 427 – 430

cm^{-1} according to the different CCSD(T) anharmonic force field calculation carried out. Its harmonic intensity varies from 1.58 km mol^{-1} (at fc-CCSD(T)/VTZ level) up to 1.86 km mol^{-1} (at CCSD(T)/CVTZ-ACVTZ(F) level), while with the anharmonic corrections taken into account it lies between 1.64 and 1.72 km mol^{-1}, in rather good agreement with the experimental value of 1.63 km mol^{-1}. The signals of the hot band $\nu_8+\nu_9-\nu_9$ at 432.9 cm^{-1} yield an experimental value for the anharmonic constant $x_{8,9}$ of 0.7 cm^{-1}, which is consistent with that computed (1.0 cm^{-1} at CCSD(T)/CVTZ-ACVTZ(F) level). The ν_{12} fundamental at 514.7 cm^{-1} is very well predicted by CCSD(T)/CVTZ-ACVTZ(F) anharmonic force field (515.5 cm^{-1}); concerning the intensity, the HYB-B2PLYP-2 hybrid, which employs the harmonic value computed at fc-CCSD(T)/ANO2 level corrected by anharmonic terms calculated at B2PLYP/CVTZ-ACVTZ(F) level, yields a final value of 1.02 km mol^{-1}, which agrees remarkable well with the observed value of 0.94 km mol^{-1} (the predictions of HYB-MP2-1 and HYB-B2PLYP-1 are slightly worse, being 0.79 and 0.73 km mol^{-1}, respectively, while HYB-MP2-2 gives 1.08 km mol^{-1}).

3.2.4. Assignments in the 600 – 1000 cm^{-1}. This spectral range comprises the ν_7, ν_{10} and ν_6 fundamentals, the weak signals coming from the first overtone of ν_9 and ν_8, and some combination and hot bands (originating from the thermally populated $\nu_9 = 1$ state). As previously described, the strong signal of ν_7 (A' symmetry) located at 700.3 cm^{-1} (in good agreement with the predicted value of 696.7 cm^{-1} computed at CCSD(T)/CVTZ-ACVTZ(F) level of theory) hides the weak feature of ν_{11} (which our anharmonic calculations predict around 708 cm^{-1} and very weak). The absorptions at 835.5 and 947.7 cm^{-1} are assigned to ν_{10} (A" symmetry) and ν_6 (A' symmetry) , respectively, as confirmed by calculations (calculated value 834.6 cm^{-1} and 944.7 cm^{-1} at CCSD(T)/CVTZ-ACVTZ(F) level of theory, respectively). The strongest band is ν_{10}, while ν_6 and ν_7 are almost equal. In addition, the analysis of the spectra recorded at higher pressure and at different resolution in order to maximize the signal-to-noise ratio led to the identification of the weak signals (predicted intensities lower than 0.1 km mol^{-1}) related to $2\nu_9$ (at 741.7 cm^{-1}) and $2\nu_8$

(at 860.3 cm^{-1}), visible in the spectra recorded at higher pressure, together with the binary combination $\nu_9+\nu_{12}$ (located at 896.2 cm^{-1}), and some hot bands involving the $v_9 = 1$ vibrational level.

3.2.5. Assignments in the 1000 – 1800 cm^{-1}. This spectral region is dominated by the strong features of ν_5 and ν_3 (both of A' symmetry), located at 1188.1 and 1655.8 cm^{-1}, respectively. As previously described, the latter is strongly perturbed by Fermi type I resonance with the nearby $2\nu_{10}$ (observed at 1689.6 cm^{-1}), and only the anharmonic data computed at CCSD(T)/CVTZ-ACVTZ(F) level correctly describes this interaction. The corresponding matrix has the following off-diagonal coupling term

$$\left\langle v_3 + 1, v_{10} \mid \hat{H} \mid v_3, v_{10} + 2 \right\rangle = \frac{\phi_{3,10,10}}{4} \qquad (2)$$

After diagonalization, the lower $v_3=1$ level (1670.3 cm^{-1}) is shifted downward to 1653.6 cm^{-1} while the vibrational $v_{10} = 2$ state moves from 1674.7 up to 1691.3 cm^{-1}, thus resulting in very good agreement with the experimental data. In the spectra recorded at higher pressure, the absorption due to the other fundamental falling in this range, the weak ν_4 band, becomes visible (centered at 1374.7 cm^{-1}). Together with the combination $\nu_{10}+\nu_{12}$ (located at 1338.1 cm^{-1}) and the first overtone of ν_7 and ν_{11}, it constitutes a tetrad of bands, $\nu_4/\nu_{10}+\nu_{12}/2\nu_7/2\nu_{11}$, which are perturbed by three Fermi resonances (one of Type I and two of Type II) and three Darling Dennison resonances (one of the 2-2 Type and two of 2-11 Type). The off-diagonal elements of the corresponding interacting matrices are:

$$\left\langle v_4 + 1, v_{10}, v_{12} \mid \hat{H} \mid v_4, v_{10} + 1, v_{12} + 1 \right\rangle = \frac{\phi_{4,10,12}}{\sqrt{8}} \qquad (3)$$

$$\left\langle \mathrm{v}_4+1,\mathrm{v}_7 \mid \hat{H} \mid \mathrm{v}_4,\mathrm{v}_7+2 \right\rangle = \frac{\phi_{4,7,7}}{4} \tag{4}$$

$$\left\langle \mathrm{v}_4+1,\mathrm{v}_{11} \mid \hat{H} \mid \mathrm{v}_4,\mathrm{v}_{11}+2 \right\rangle = \frac{\phi_{4,11,11}}{4} \tag{5}$$

$$\left\langle \mathrm{v}_7+2,\mathrm{v}_{11} \mid \hat{H} \mid \mathrm{v}_7,\mathrm{v}_{11}+2 \right\rangle = \frac{K_{7,7;11,11}}{2} \tag{6}$$

$$\left\langle \mathrm{v}_7+2,\mathrm{v}_{10},\mathrm{v}_{12} \mid \hat{H} \mid \mathrm{v}_7,\mathrm{v}_{10}+1,\mathrm{v}_{12}+1 \right\rangle = \frac{K_{7,7;10,12}}{\sqrt{8}} \tag{7}$$

$$\left\langle \mathrm{v}_{11}+2,\mathrm{v}_{10},\mathrm{v}_{12} \mid \hat{H} \mid \mathrm{v}_{11},\mathrm{v}_{10}+1,\mathrm{v}_{12}+1 \right\rangle = \frac{K_{11,11;10,12}}{\sqrt{8}} \tag{8}$$

The magnitude of the effects of Fermi resonances on the values of the different Darling-Dennison constants involved in the calculation of the matrix elements can be evaluated by computing the corresponding values keeping the resonance denominators and comparing them with those obtained after their removal. For $K_{7,7;10,12}$ and $K_{7,7;11,11}$ the effects are dramatic: the perturbed values ($K_{7,7;10,12}$ = 474.76 cm^{-1}, $K_{7,7;11,11}$ = 330.29 cm^{-1}) are two order of magnitude larger than the deperturbed ones ($K_{7,7;10,12}$ = –0.53 cm^{-1}, $K_{7,7;11,11}$ = –2.80 cm^{-1}). Concerning $K_{11,11;10,12}$ taking into account FR lowers its value from 16.40 cm^{-1} to 1.04 cm^{-1}. Once the correct values for the Darling-Dennison constants were obtained, this polyad (and the followings) was used to evaluate the criteria, recently suggested,[72] for selecting the DDR resonances which are mandatory to treat by post-VPT2 variational procedure. Krasnoshchekov[72] suggested the need to consider the couplings which: (1) have a value of the coupling term greater than 5.0 cm^{-1}; (2) the resonance denominator containing the corresponding harmonic frequencies of the involved levels is less than 200 cm^{-1}; and (3) the so-called repulsion effect, ε_{1-2}, occurring on the two deperturbed vibrational levels as a consequence of diagonalization of the corresponding block Hamiltonian matrix, is larger than 0.1 cm^{-1}. The latter term is computed by using the following expression:[72]

$$\varepsilon_{1-2} = \frac{|E_2 - E_1|}{2}\left[\sqrt{1+\frac{4K^2}{(E_2 - E_1)^2}} - 1\right] \quad (9)$$

where K is the coupling terms between the two deperturbed (i.e. computed by using the $x^*_{i,j}$ anharmonicity constants) vibrational levels E_1 and E_2. Besides, Krasnoshchekov compared these criteria to the one based on the ratio, P, of the coupling coefficient to the energy difference between the involved vibrational levels: a value close to (or larger than) 0.1 points to the presence of a resonance which should be explicitly taken into account.[107] The larger ε_{1-2} value (0.17 cm^{-1}) is computed for the $2\nu_7/2\nu_{11}$, thus suggesting the relevance of this interactions with respect to the other two DDR (being ε_{1-2} = 0.04 and 0.01 cm^{-1} for $2\nu_{11}/\nu_{10}+\nu_{12}$ and $2\nu_7/\nu_{10}+\nu_{12}$, respectively). Looking at the P values, that of $2\nu_7/2\nu_{11}$ is 0.0831, larger than those for the other two DDR (0.019 and 0.024 for $2\nu_{11}/\nu_{10}+\nu_{12}$ and $2\nu_7/\nu_{10}+\nu_{12}$, respectively), thus being in line with the indications yielded by considering ε_{1-2} parameter. Considering the complete matrix (containing all the DDR plus the Fermi resonances), after its diagonalization the corresponding eigensolutions are ν_4 = 1376.8 cm^{-1} (moved upward of 4.6 cm^{-1}), $\nu_{10}+\nu_{12}$ = 1338.7 cm^{-1} (shifted downward of about 14 cm^{-1}) , $2\nu_7$ = 1391.2 cm^{-1} and $2\nu_{11}$ = 1424.6 cm^{-1} (moved up by about 10 cm^{-1}). These predictions are in a very good agreement with the experimentally measured values of 1338.1 cm^{-1} ($\nu_{10}+\nu_{12}$) and 1374.7 cm^{-1} (ν_4). Neglecting the anharmonic couplings involving $2\nu_{11}/\nu_{10}+\nu_{12}$ and $2\nu_7/\nu_{10}+\nu_{12}$ the eigensolutions are ν_4 = 1377.5, $\nu_{10}+\nu_{12}$ = 1338.4, $2\nu_7$ = 1391.2 and $2\nu_{11}$ = 1424.3 cm^{-1}. As it can be seen, the differences for $2\nu_{11}$, $2\nu_7$ and $\nu_{10}+\nu_{12}$ are small (less than 0.3 cm^{-1}), but for ν_4 the predictions are significantly different (2.8 cm^{-1}), as a consequence of its complex interactions with the other vibrational states.

The remaining absorptions visible in the spectra at higher pressure are due to two quanta combination bands and first overtones, and their measured positions are all consistent with their

corresponding predicted values (the mean of the absolute deviations between observed and predicted transitions, MAD, is 2.4 cm^{-1}).

3.2.6. Assignments in the 1800 – 2900 cm^{-1}. The analysis of this spectral region was carried out on the spectra recorded at higher pressure, since it is characterized by the weak absorptions due to binary combination bands and first overtones. The latter are $2\nu_6$ (located at 1893.9 cm^{-1}) and $2\nu_5$ (at 2370.4 cm^{-1}) in rather good agreement with their theoretical values of 1887.5 and 2362.8 cm^{-1}, respectively. Between them, the most important features is assigned to $\nu_5+\nu_6$ (at 2130.2 cm^{-1}), with a predicted intensity quite similar to those predicted for $2\nu_6$ and $2\nu_5$. At higher wavenumbers there is a complex structure arising from the overlapped absorptions of different weak two quanta ($\nu_4+\nu_5$, $\nu_3+\nu_6$, $\nu_3+\nu_5$) and three quanta combination bands ($\nu_3+2\nu_8$, $\nu_3+2\nu_{12}$). For this spectral region, the overall agreement with the calculated band positions could be considered more than satisfactory (MAD = 6.5 cm^{-1}).

3.2.7. Assignments in the 2900 – 3200 cm^{-1}. As previously described, in this interval we locate the ν_1 and ν_2 fundamentals at 3158.9 and 3072.1 cm^{-1}, respectively, revising the previously assignments. The ν_1 fundamental is essentially free from anharmonic interactions with nearby vibrational states. The ν_2 band is perturbed by a Fermi Type II resonance with the nearby $\nu_3+\nu_4$, observed at 3020.2 cm^{-1}; the corresponding off-diagonal coupling term has the following form

$$\left\langle \mathrm{v}_2+1, \mathrm{v}_3, \mathrm{v}_4 \mid \hat{H} \mid \mathrm{v}_2, \mathrm{v}_3+1, \mathrm{v}_4+1 \right\rangle = \frac{\phi_{2,3,4}}{\sqrt{8}} \qquad (10)$$

and the eigensolutions of the resulting matrix are ν_2 = 3081.0 cm^{-1} and $\nu_3+\nu_4$ = 3014.5 cm^{-1}. This kind of coupling between the levels of the symmetric CH_2 stretching and binary combination related to C=C stretching and CH_2 scissor mode is common to other ethenic compounds.[47, 108]

In addition, in the spectra (see Figure 4) there is partially visible another signal (shoulder around 3102 cm^{-1}) which, on the basis of its expected (deperturbed) value and taking into account the intensity, can be tentatively assigned to $\nu_3+2\nu_{11}$, a three quanta combination band involving the strong ν_3 fundamental. Taking into account the corresponding anharmonic resonance leads to the following Darling-Dennison coupling terms to be considered:

$$\left\langle \mathrm{v}_2, \mathrm{v}_3+1, \mathrm{v}_{11}+2 \,|\, \hat{H} \,|\, \mathrm{v}_2+1, \mathrm{v}_3, \mathrm{v}_{11} \right\rangle = \sqrt{2}\,\frac{K_{2;11,11,3}}{4} \qquad (11)$$

The eigensolutions of the corresponding polyad are $\nu_3+\nu_4$ = 3011 cm^{-1}, ν_2 = 3071.6 cm^{-1}, and $\nu_3+2\nu_{11}$ = 3094.6 cm^{-1}, in rather good agreement with the measured spectroscopic values. Also in this case neglecting of Fermi resonances yields abnormally large values for the K_{DD} constant: the $K_{2;11,11,3}$ term becomes 36.26 cm^{-1} (perturbed) instead of –0.14 cm^{-1} (deperturbed). The analysis of this polyad suggests that the DDR coupling between $\nu_3+2\nu_{11}$ and ν_2 is very low ($\varepsilon_{1-2} \approx 0$ cm^{-1}, *P*-ratio = 0.0022). A similar mixing (due to anharmonic resonances) with other vibrational states concerning the CH_2 stretching falling at lower frequency, while the one located at higher wavenumbers is essentially unperturbed, has been detected and analyzed for 1,1-difluoroethene.[39]

3.2.8. Assignments in the 3200 – 5900 cm^{-1}. The observed absorptions falling in this spectral interval are binary combination bands mostly involving ν_1 and ν_2 vibrational levels, some ternary combinations (visible only in the spectra recorded at higher pressure), and the first and second overtones of ν_3 (measured at 3325.9 and 4969.7 cm^{-1}, respectively). The predicted band centers agree reasonably well with the spectroscopic data (MAD of 7.0 cm^{-1}).

3.2.9. Assignments in the 5900 – 6400 cm^{-1}. This spectral region is characterized (see Figure 5) by the absorptions of the first overtones of CH_2 stretchings ($2\nu_1$ and $2\nu_2$, observed at 6272.6 and 6042.6 cm^{-1}, respectively); together with the binary combination $\nu_1+\nu_2$ (measured at

6106.2 cm^{-1}) they constitute a triad coupled by three Darling-Dennison resonances (one of the 2-2 Type and two of the 1-1 Type). The corresponding off-diagonal terms are:

$$\left\langle \mathrm{v}_1+2,\mathrm{v}_2 \mid \hat{H} \mid \mathrm{v}_1,\mathrm{v}_2+2 \right\rangle = \frac{K_{1,1;2,2}}{2} \tag{12}$$

$$\left\langle \mathrm{v}_1+1,\mathrm{v}_2 \mid \hat{H} \mid \mathrm{v}_1,\mathrm{v}_2+1 \right\rangle = \frac{\sqrt{2}}{2}\left[3K_{1,1;2,1} + \frac{3}{2}K_{1,2;2,2} + \frac{1}{2}\sum_{l\neq 1,2} K_{1,l;2,l} \right] \tag{13}$$

$$\left\langle \mathrm{v}_1,\mathrm{v}_2+1 \mid \hat{H} \mid \mathrm{v}_1+1,\mathrm{v}_2 \right\rangle = \frac{\sqrt{2}}{2}\left[3K_{2,2;1,2} + \frac{3}{2}K_{2,1;1,1} + \frac{1}{2}\sum_{l\neq 1,2} K_{2,l;1,l} \right] \tag{14}$$

As previously done for the other polyads, also this one was analyzed to determine the relative relevance of the different DDR involved. The 2-2 resonance involving $2\nu_1/2\nu_2$ has ε_{1-2} = 16.04 cm^{-1} and a *P*-ratio of 0.30, while the other two couplings (1-1 DDR) have smaller values ($2\nu_1/\nu_1+\nu_2$, ε_{1-2} = 3.68 cm^{-1}, *P*-ratio = 0.27; $2\nu_2/\nu_1+\nu_2$, ε_{1-2} = 2.75 cm^{-1}, *P*-ratio = 0.14). These results suggest that the stronger perturbation is due to the 2-2 DDR between v_1 = 2 and v_2 = 2 vibrational states. Taking into account all the anharmonic resonances, the v_2 = 2 vibrational state is moved down by about 17 cm^{-1}, the v_1 = 2 is shifted upward by about 20 cm^{-1}, while the $\nu_1+\nu_2$ state is perturbed by only 2 cm^{-1}. The eigensolutions of the resonant matrix containing all the coupling terms are $2\nu_1$ = 6273.2 cm^{-1}, $2\nu_2$ = 6041.7 cm^{-1}, and $\nu_1+\nu_2$ = 6109.7 cm^{-1}, thus being in remarkable agreement with the spectroscopic data. The overall agreement between experimental and theoretical values (MAD = 4.0 cm^{-1}) is very good. In this case the error caused by terms affected by Fermi resonances yields some differences (up to a few cm^{-1}) in some of the $K_{1,l;2,l}$ and $K_{2,l;1,l}$ involved in the sum related to the 1-1 resonances between $\nu_1+\nu_2$ and the first overtones of ν_1 and ν_2.

Table 5 summarizes all the assignments carried out in the present work, together with their estimated experimental errors; where identifiable, the absorptions related to ^{37}ClFC=CH$_2$ are also listed. The overall assignments are consistent with the predicted values, and the small value of the

absolute mean deviations for the transitions. For the data computed at CCSD(T)/CVTZ-ACVTZ(F) level of theory, considering the reduced set containing only fundamentals, first overtones and binary bands the MAD is 4.6 cm^{-1}, while taking into account the overall set it becomes 5.3 cm^{-1}; this value confirms the quality of the anharmonic force field calculation carried out in this work.

In Table 6 are reported the fundamental modes together with their theoretical values computed by the anharmonic force fields at CCSD(T)/CVTZ-ACVTZ(F) level of theory and employing the GVPT2 as well as the HDCPT2 approaches for treatment of resonant terms. Concerning the GVPT2 model, the deviations between the experimental and the corresponding theoretical values lie within 3 cm^{-1}: this agreement is remarkable (mean absolute deviation of 2.0 cm^{-1}) thus assessing the high quality of the *ab initio* force field. In addition, for the ν_9 and ν_{11} fundamental modes, which could not be identified in the experimental spectrum due to their too weak intensities, one can rely on the computed values. Three resonance manifolds were identified from which significant perturbations of the fundamental levels of ν_2, ν_3 and ν_4 originate. Their values, marked with an asterisk in Table 6, are the eigensolutions of the corresponding resonant matrices and are also in good agreement with the experimental data. The HDCPT2 model with the same basis set and level of theory yields rather satisfactory results (almost all the predictions lie within 10 cm^{-1} with respect to their experimental counterparts), except the ν_3 fundamental, which is strongly perturbed by Fermi Type I interaction with $2\nu_{10}$ and several Darling-Dennison resonances (as previously discussed). It is interesting to compare these performances obtained at CCSD(T) level of theory with those yielded by the hybrids HYB-MP2-1 and HYB-B2PLYP-1 (which have the harmonic data at CCSD(T) level and the anharmonic ones at MP2 and B2PLYP level, respectively) thus assessing the accuracy of their cubic and quartic semi diagonal force constants. Within the framework of GVPT2 model, the fundamentals predicted by HYB-MP2-1 have a MAD of 3.8 cm^{-1}, with a maximum deviation of 6.3 cm^{-1}, while the theoretical data computed by HYB-B2PLYP-1 show a MAD of 3.3 cm^{-1}, with a maximum discrepancy of 6.2 cm^{-1}. The HDCPT2

approach yields a MAD of 5.6 cm^{-1} and 6.1 cm^{-1} for HYB-MP2-1 and HYB-B2PLYP-1, respectively, the maximum deviation for both being the predicted value of ν_3 (which is computed about 30 cm^{-1} higher than the experimental observation). By considering these overall results, the good performances of B2PLYP model for computing anharmonic corrections within GVPT2 approach are further confirmed.

In Table 7 the left lower triangle of the symmetric matrix formed by the computed anharmonicity constants, $x_{i,j}$, is reported. The calculated values which are affected by Fermi interactions are labeled by an asterisk: in these cases it is necessary to consider the $x_{i,j}$ effective constants excluding the contributions of the interacting vibrations from the perturbational summations.[91] These effective anharmonicity constants were here introduced to account for the following Fermi resonances: $\nu_2/\nu_3+\nu_4$, $\nu_3/2\nu_{10}$, and $\nu_4/\nu_{10}+\nu_{12}/2\nu_7/2\nu_{11}$. The symmetric and asymmetric CH_2 stretching vibrations of the ethene group follow the *x-K* relations of Mills and Robiette[109] here reported

$$x_{1,1} = x_{2,2} = x_{1,2}/4 = K_{1,1;2,2}/4 \quad (15)$$

where $K_{1,1;2,2}$ is the Darling-Dennison constant. The corresponding calculated theoretical values (in units of cm^{-1}) are $x_{1,1} = -32.7$, $x_{2,2} = -28.4$, $x_{1,2} = -105.4$, and $K_{1,1;2,2} = -116.35$, in good agreement with the empirical relations. In general, most of the experimentally derived anharmonic constants are consistent with respect to their theoretical counterparts (derived from VPT2 calculations carried out), thus further supporting the overall vibrational assignment. The presence of several anharmonic resonances (previously discussed) explains the observed deviations between the computed and the experimental anharmonic constants; in particular, Fermi and Darling Dennison resonances involving ν_3 and ν_2 are reflected by the spread between the calculated and observed parameters (which were derived from the position of binary combination and the corresponding fundamentals),

especially for the $x_{2,2}$, $x_{2,6}$, $x_{3,4}$, $x_{3,5}$, $x_{3,6}$, $x_{3,10}$, and $x_{3,12}$ ones. In these cases the experimental values should be taken as effective fitting parameters, thus not being comparable with the anharmonicity constants derived from perturbation theory. The effect of the Fermi resonance concerning the ν_3 can be clearly seen by looking at the $x_{3,3}$ constant. The value of $x_{3,3}$ determined taking into account the experimental positions of its first and second overtones agrees very well with the theoretical predictions, since $2\nu_3$ and $3\nu_3$ are not affected by anharmonic resonances. On the other hand, the one yielded by the analysis of $2\nu_3$ and ν_3 is clearly affected by the interaction of the latter with the $\nu_{10} = 2$ vibration level (Fermi type I resonance, as previously discussed in the text).

3.3. Theoretical calculations of molecular spectroscopic parameters

Once the rotational constants related to the equilibrium structure were determined, those of the vibrational ground state were subsequently computed by taking into account the corresponding vibrational corrections given by computed anharmonic vibration-rotation α constants. Quartic centrifugal distortion constants were obtained from the harmonic force field data, while sextic centrifugal distortion terms were calculated on the basis of the cubic force constants. To obtain the vibrational corrections to rotational constants and the sextic centrifugal distortion parameters for both $^{35}ClFC=CH_2$ and $^{37}ClFC=CH_2$, once the complete anharmonic force field up to the third order were obtained, it was transformed from the dimensionless normal coordinate space into the internal coordinate representation. The internal quadratic and cubic force constants, where no masses enter in their definition, were then used for computing the molecular spectroscopic parameters, relevant to rotational spectroscopy, of either ^{35}Cl-isotopologue or ^{37}Cl-isotopologue of 1-chloro-1-fluoroethene. Table 8 lists the calculated anharmonic vibration-rotation α constants. Within the VPT2 approach the computation of these data could be affected by Coriolis resonances and therefore we checked for the presence of these kind of couplings. We found that there is a

significant *a*-axis coupling between the $v_7 = 1$ and $v_{11} = 1$ vibrational modes, and therefore for the calculation of the corresponding α constants we followed the procedure suggested by Papoušek and Aliev.[91] Table 8 lists also the available experimental data: the overall agreement with the theoretical values should be considered more than satisfactory. Table 9 reports the results (rotational ground state constants, quartic and sextic centrifugal distortion terms) obtained by using the CCSD(T)/CVTZ-ACVTZ(F) level of theory. Here the computed ground state rotational and quartic centrifugal distortion constants are compared with the recent experimental data yielded by Leung *et al.*,[54] while the calculated sextic distortion terms are compared with the values reported by Alonso *et al.*[51] Concerning the ground state rotational constants, the predicted values differ less than 0.7% with respect to the microwave data,[54] with a mean accuracy of 0.6% for both the chlorine isotopologues. Moving to the centrifugal distortion terms, the quartic ones (for both the ^{35}Cl and ^{37}Cl isotopologues) are computed with a mean deviation of 1.8% with respect to the most recent values, while for the sextic constants the discrepancies are generally within 20% for ^{35}ClFC=CH$_2$ (MAD of 15%), while the predictions for ^{37}ClFC=CH$_2$ show larger discrepancies, especially for ϕ_{JK} and Φ_J. To comment these results, we highlight that the experimental accuracy for ^{35}ClFC=CH$_2$ and ^{37}ClFC=CH$_2$ sextic fitted parameters is not very high, being the standard errors for the former in the range 3% (ϕ_K) to 18% (Φ_{KJ}) and those of the latter from 6% (Φ_K) to 25% for ϕ_{JK} (considering 3 times the standard deviation, this interval becomes 18% – 75%); besides, the same authors pointed out that some of the centrifugal distortion constants are strongly correlated.[51]

Table 9 lists also the diagonal elements of the inertial chlorine quadrupole coupling tensor χ_{ij} obtained at CCSD(T)/CVTZ-ACVTZ(F) level of theory; the elements of the tensor, evaluated from an applied field gradient q_{ij}, were calculated according the relation

$$\chi_{ij} = e\,Q\,q_{ij} \qquad (i, j = a, b, c) \tag{16}$$

where *e* is the electronic charge, *Q* the nuclear electric quadrupole moment of chlorine nucleus, and *a*, *b*, and *c* are the inertial axes. Being 1-chloro-1-fluoroethene a planar molecule, the inertial nuclear quadrupole tensor has only one off-diagonal element, χ_{ab}. Using $Q(^{35}\mathrm{Cl})$ = –0.08165 barn and $Q(^{37}\mathrm{Cl})$ = –0.06435 barn (both values taken from Ref. 110), the nuclear quadrupole coupling tensors were computed as

$$\chi_{ij}\ (\mathrm{MHz}) = 234.9647\ Q\ (\mathrm{barn})\ q_{ij}\ (\mathrm{au}) \qquad (i, j = a, b, c) \tag{17}$$

3.4. Cross Section Spectra and Computed Anharmonic Dipole Moment Surface.

In the present work, besides the thorough vibrational assignments previously reported, accurate measurements of integrated band intensities were carried out on the corresponding absorption cross section spectrum. These data, necessary to quantify the impact of halocarbons on the Earth's radiative budget, are also required to thoroughly evaluate the quality of the computed anharmonic dipole moment surface. Several spectra were measured at increasing sample pressures and employing N_2 as inert buffer gas: the analysis on this series of measurements was then carried out by using an established procedure where, assuming the validity of Beer's law, the point-by-point absorbance value $A(\tilde{\nu})$ measured at each wavenumber, $\tilde{\nu}$, was least square fitted versus the corresponding gas concentration. From this regression analysis it was therefore derived the slope $\sigma(\tilde{\nu})$ at each wavenumber; this slope is the absorbance cross section per molecule (cm^2 $\mathrm{molecule}^{-1}$) according to

$$\sigma(\tilde{\nu}) = \frac{A(\tilde{\nu})\ln(10)}{N_A c l} \tag{18}$$

where *l* is the optical path length (cm), *c* corresponds to the sample concentration (mol cm^3) and N_A is the Avogadro's constant. As noted in our previous studies[76] this approach, proposed by Chu *et al.*,[111] offers the great advantage of using a wide range of sample pressure by avoiding distortion in the measured absorbance values related to saturation effects for the stronger bands and therefore it greatly improves the signal-to-noise ratio for the weaker signals; besides this method also yields the error estimate at each wavenumber in terms of the statistical uncertainty given by the fitting procedure. Figure 6 shows the absorption cross section spectrum of 1-chloro-1-fluoroethene in the 400 – 6400 cm^{-1} range; as it can be seen, the most intense absorptions fall between 1000 and 1800 cm^{-1}, being related to ν_5 and ν_3 fundamentals.

As reported in the previous section, the CCSD(T) harmonic intensities obtained in conjunction with the CVTZ-ACVTZ(F) and ANO2 basis sets were corrected by means of anharmonic corrections calculated at the B2PLYP and MP2 levels of theory employing the CVTZ-ACVTZ(F) basis set, thus leading to the different hybrid models HYB-MP2-1, HYB-B2PLYP-1, HYB-MP2-2 and HYB-B2PLYP-2. For the calculation carried out with B2PLYP functionals, we tested also the influence of the integration grids available in Gaussian09 on the computed anharmonic corrections to intensities. Since we found a negligible difference between the result obtained with *SuperFine* (150 radial points, 794 angular points) grid and the one yielded by *UltraFine* (99 radial points, 590 angular points), we employed the *UltraFine* grid for computing the anharmonic corrections to CCSD(T) harmonic intensities. Table 10 reports the experimental integrated absorption cross section values (and the corresponding integration limits) and the computed data. There is an overall good agreement between the measured data and the computed values for all the different hybrid models employed (the mean absolute error is less than 1.20 km mol^{-1} for all the three calculations). The best performances are yielded by combining the anharmonic corrections at B2PLYP level with the harmonic intensities at CCSD(T) level of theory and in conjunction with the CVTZ-ACVTZ(F) basis set (mean absolute deviation of 0.60 km mol^{-1} considering the whole spectral region up to 6400 cm^{-1}) while those of HYB-MP2-1 are

slightly worse (MAD of 0.69 km mol^{-1}). Using the harmonic data yielded by ANO2 basis, the MAD are 0.99 and 0.91 km mol^{-1} for HYB-MP2-2 and HYB-B2PLYP-2, respectively. On these grounds, we can conclude that B2PLYP yields anharmonic corrections to intensities which result in better agreement with the experimental data, thus further confirming the reliability of this DFT method, especially when employed in conjunction with the harmonic data provided by calculations carried out at higher level of electronic correlation.

4. CONCLUSIONS

In this work, we presented a complete analysis of the gas-phase infrared spectra of 1-chloro-1-fluoroethene up to 6400 cm^{-1} supported by high-level *ab initio* computations. Accurate band position values for fundamentals, overtones, and combination bands up to three quanta were determined. Besides this vibrational investigation, the absorption cross section spectra were measured over the 400 – 6400 cm^{-1} spectral region and the integrated band intensities for the most important absorption features were determined with a great accuracy. Harmonic calculations at CCSD(T) level of theory and employing different basis sets were carried out to provide optimized geometries and the corresponding quadratic force field data for both frequencies and intensities, plus the quartic centrifugal distortion constants. Within the framework of GVPT2, the cubic and quartic semi-diagonal force constants obtained using different basis sets were then employed to compute the theoretical predictions of the anharmonic spectra. The best agreement between experimental and theoretical positions was reached by the anharmonic force field at CCSD(T) level of theory and employing the CVTZ-ACVTZ(F) basis set, which uses the correlation consistent polarized core/valence triple zeta basis set cc-pCVTZ[79,83,84] for Cl, C and the aug-cc-pCVTZ[80,84] basis set for the F atom to correctly describe the issues related to the π charge distribution of haloethenes.[82] The analysis led to the identification of many polyads affected by Fermi (both type I

and II) and several Darling-Dennison (2-2, 2-11, 1-21, 1-3, 1-1) resonances. Concerning the latter, the removal of the terms related to resonance denominators was found to be mandatory for a correct evaluation of the DDR couplings and for assessing their relative magnitude. The computed values obtained from the diagonalization of the corresponding interaction matrices were found in very good agreement with the experimental counterparts (for the whole set of transitions the mean absolute deviation is 5.3 cm^{-1}) thus confirming the quality of the *ab initio* calculations. Accurate values for integrated cross sections were determined for all the most important absorptions falling in the range 400 – 6400 cm^{-1}; these data were used to assess the performances of MP2 and B2PLYP methods in computing anharmonic corrections to harmonic intensities. The comparison confirms the overall good performances of the B2PLYP functional especially when used in conjunction with the harmonic data obtained by calculations carried out at higher level of electronic correlation.

Acknowledgments

This work has been supported by MIUR (PRIN 2012 funds for project "STAR: Spectroscopic and computational Techniques for Astrophysical and atmospheric Research", prot. no. 20129ZFHFE_003) and by University Ca' Foscari Venezia (ADIR funds). The High Performance Computing department of the CINECA Supercomputer Centre (Grant No. HP10C292PO) and the SCSCF ("*Sistema per il Calcolo Scientifico di Ca' Foscari*") facility are gratefully acknowledged for the utilization of computer resources.

REFERENCES

(1) Mattes, E. T.; Alexander, A. K.; Coleman, N. V. Aerobic biodegradation of the chloroethenes: pathways, enzymes, ecology, and evolution. *Microb. Reviews* **2010**, 34, 445–475.

(2) Dobrzyńska, E.; Pośniak, M.; Szewczyńska, M.; Buszewski, B. Chlorinated Volatile Organic Compounds—Old, However, Actual Analytical and Toxicological Problem. *Crit. Reviews in Anal. Chemistry*, **2010**, 40, 41–57.

(3) van Hylckama Vlieg, J. E. T.; Janssen, D. B. Formation and Detoxification of Reactive Intermediates in the Metabolism of Chlorinated Ethenes. *J. Biotech.* **2001**, 85, 81–102.

(4) McNaughton, D.; Robertson, E.G.; Thompson, C.D.; Chimdi, T.; Bane, M.K. Appadoo, D. Overview of High-Resolution Infrared Measurement and Analysis for Atmospheric Monitoring of Halocarbons. *Anal. Chem.* **2010**, 82, 7958–7964.

(5) Tasinato, N.; Stoppa, P.; Pietropolli Charmet, A.; Giorgianni, S.; Gambi, A. Modelling the Anharmonic and Coriolis Resonances Within the Six Level Polyad Involving the ν_4 Fundamental in the Ro-vibrational Spectrum of Vinyl Fluoride. *J. Quant. Spectrosc. Radiat. Transfer* **2012**, 113, 1240–1249.

(6) Visinoni, R.; Stoppa, P.; Pietropolli Charmet, A.; Giorgianni, S.; Nivellini, G.D. High-Resolution FTIR Analysis of the $2\nu_6$ Overtone of cis-CHF–CHF and Fermi Resonance Study with the ν_2 Fundamental. *Chem. Phys. Lett.* **2005**, 416, 293–299.

(7) Stoppa, P.; Pietropolli Charmet, A.; Visinoni, R.; Giorgianni, S. Laser Infrared Spectroscopy of Vinyl Fluoride in the 1280-1400 cm^{-1} Region. *Mol. Phys.* **2005**, 103, 657–666.

(8) Robertson, E.G.; Thompson, C.D.; Appadoo, D.; McNaughton, D. Tetrafluoroethylene: High Resolution FTIR Spectroscopy. *Phys. Chem. Chem. Phys.* **2002**, 4, 4849-4854.

(9) Fuss, W.; Robertson, E.G.; Medcraft, C.; Appadoo, D.R.T. Vibrational Anharmonicities and Reactivity of Tetrafluoroethylene. *J. Phys. Chem. A* **2014**, 118, 5391–5399.

(10) Robertson, E.G.; Medcraft, C.; McNaughton, D.; Appadoo, D. The Limits of Rovibrational Analysis: The Severely Entangled ν_1 Polyad Vibration of Dichlorodifluoromethane in the Greenhouse IR Window. *J. Phys. Chem. A* **2014**, 118, 10944-10954.

(11) Medcraft, C.; Fuss, W.; Appadoo, D.R.T.; McNaughton, D.; Thompson, C.D.; Robertson, E.G. Structural, Vibrational, and Rovibrational Analysis of Tetrafluoroethylene. *J. Chem. Phys.* **2012**, 137, 214301.

(12) Wugt Larsen, R.; Hegelund, F.; Engdahl, A.; Uvdal, P.; Nelander, B. High-Resolution Infrared Study of Collisionally Cooled trans-1,2-Dichloroethylene. *J. Mol. Spectrosc.* **2007**, 243, 99–102.

(13) Albert, S.; Baurecker, S.; Quack, M.; Steinlin, A. Rovibrational Analysis of the $2\nu_3$, $3\nu_3$ and ν_1 Bands of $CHCl_2F$ Measured at 170 and 298 K by High-Resolution FTIR Spectroscopy. *Mol. Phys.* **2007**, 105, 541–558.

(14) Thompson, C.D.; Robertson, E.G.; McNaughton, D. Completing the Picture in the Rovibrational Analysis of Chlorodifluoromethane ($CHClF_2$): ν_3 and ν_8. *Mol. Phys.* **2004**, 102, 1987–1695.

(15) Bauerecker, S.; Taraschewski, M.; Weitkamp, C.; Cammenga, H.K. Liquid-helium Temperature Long-Path Infrared Spectroscopy of Molecular Clusters and Supercooled Molecules. *Rev. Sci. Instrum.* **2001**, 72, 3946–3955.

(16) Canè, E.; Villa. M.; Tamassia, F.; Pietropolli Charmet, A.; Tasinato, N.; Stoppa, P.; Giorgianni, S. The Ro-Vibrational Analysis of the ν_4 Fundamental Band of CF_3Br from Jet-Cooled Diode Laser and FTIR Spectra in the 8.3μm Region. *Mol. Phys.* **2014**, 112, 1899–1909.

(17) Brumfield, B.E.; Stewart, J.T.; Widicus Weaver, S.L.; Escarra, M.D.; Howard, S.S.; Gmachl, C.F.; McCall, B.J. A Quantum Cascade Laser Cw Cavity Ringdown Spectrometer Coupled to a Supersonic Expansion Source. *Rev. Sci. Instrum.* **2010**, 81, 063102.

(18) Lauro, C.; D'Amico, G.; Snels, M. Torsional Splittings in the Diode Laser Slit-Jet Spectra of the ν_6 Fundamental of 1-Chloro-1,1-Difluoroethane (HCFC-142b). *J. Mol. Spectrosc.* **2009**, 254, 108–118.

(19) Pietropolli Charmet, A.; Stoppa, P.; Toninello, P.; Baldacci, A.; Giorgianni, S. Jet-Cooled Diode Laser Spectra of CF_3Br in the 9.2 μm Region and Rovibrational Analysis of Symmetric CF_3 Stretching Mode. *Phys. Chem. Chem. Phys.* **2006**, 8, 2491–2498.

(20) Pietropolli Charmet, A.; Stoppa, P.; Toninello, P.; Giorgianni, S.; Ghersetti, S. Rovibrational Analysis of the ν_1 Fundamental of CF_3Cl from Diode Laser Spectra in a Supersonic Slit-Jet Expansion. *Phys. Chem. Chem. Phys.* **2003**, 5, 3595–3599.

(21) Herman, M.; Georges, R.; Hepp, M.; Hurtmans, D. High Resolution Fourier Transform Spectroscopy of Jet-Cooled Molecules. *Int. Rev. Phys. Chem.* **2000**, 19, 277–325.

(22) Marques, J.M.C.; Prudente, F.V.; Pereira, F.B.; Almeida, M.M.; Maniero, A.M.; Fellows, C.E. A New Genetic Algorithm to be Used in the Direct Fit of Potential Energy Curves to Ab Initio and Spectroscopic Data. *J. Phys. B: At. Mol. Opt. Phys.* **2008**, 41, 085103.

(23) Lodyga, W.; Kreglewski, M.; Pracna, P.; Urban, S. Advanced Graphical Software for Assignments of Transitions in Rovibrational Spectra. *J. Mol. Spectrosc.* **2007**, 243, 182–188.

(24) Tasinato, N.; Pietropolli Charmet, A.; Stoppa, P. ATIRS package: A Program Suite for the Rovibrational Analysis of Infrared Spectra of Asymmetric Top Molecules. *J. Mol. Spectrosc.* **2007**, 243, 148–154.

(25) Robertson, E.G.; McNaughton, D. Maximising Rovibrational Assignments in the ν_1 Band of NSCl by Spectral Analysis by Subtraction of Simulated Intensities (SASSI). *J. Mol. Spectrosc.* **2006**, 238, 56–63.

(26) Meerts, W.L.; Schmitt, M. A New Automated Assign and Analysing Method for High-Resolution Rotationally Resolved Spectra Using Genetic Algorithms. *Phys. Scripta* **2005**, 73, C47-C52.

(27) Medvedev, I.R.; Winnewisser, M.; Winnewisser, B.P.; De Lucia, F.C.; Herbst, E. The Use of CAAARS (Computer Aided Assignment of Asymmetric Rotor Spectra) in the Analysis of Rotational Spectra *J. Mol. Struct.* **2005**, 742, 229–236.

(28) Hua, L.; Lee, W-B.; Chao, M-H.; Zhang, B.; Lin, K-C. Elimination Mechanism of Br_2^+ and Br^+ in Photodissociation of 1,1- and 1,2-Dibromoethylenes Using Velocity Imaging Technique. *J. Chem. Phys.* **2011**, 134, 194312.

(29) Lee, S-H.; Chen, W.K.; Chaudhuri, C.; Huang, W-J.; Lee, Y.T. Photodissociation Dynamics of Vinyl Fluoride (CH_2CHF) at 157 and 193 nm: Distributions of Kinetic Energy and Branching Ratios. *J. Chem. Phys.* **2006**, 125, 144315, and references therein.

(30) Wu, C-Y.; Chung, C-Y.; Lee, Y-C.; Lee, Y-P. Three-Center versus Four-Center Elimination of Haloethene: Internal Energies of HCl and HF on Photolysis of CF_2CHCl at 193 nm Determined with Time-Resolved Fourier-Transform Spectroscopy. *J. Chem. Phys.* **2002**, 117, 9785–9792.

(31) Lin, S-H.; Lin, S-C.; Lee, Y-C.; Chou, Y-C.; Chen, I-C.; Lee, Y-P. Three-Center Versus Four-Center Elimination in Photolysis of Vinyl Fluoride and Vinyl Bromide at 193 nm: Bimodal Rotational Distribution of HF and HBr ($v \leq 5$) Detected With Time-Resolved Fourier Transform Spectroscopy. *J. Chem. Phys.* **2001**, 114, 7396–7406.

(32) Blanco, M.B.; Taccone, R.A.; Lane, S.I.; Teruel, M.A. Kinetics of the Reactions of $O(^3P)$ with $CCl_2=CH_2$, (Z)-CHCl=CHCl, and $CCl_2=CCl_2$: A Temperature Dependence Study. *J. Phys. Chem. A* **2006**, 110, 11091−11097.

(33) Baasandorj, M.; Knight, G.; Papadimitriou, V.C.; Talukdar, R.K.; Ravishankara, A.R.; Burkholder, J.B. Rate Coefficients for the Gas-Phase Reaction of the Hydroxyl Radical with $CH_2=CHF$ and $CH_2=CF_2$. *J. Phys. Chem. A* **2010**, 114, 4619–4633.

(34) Orkin, V.L.; Louis, F.; Huie, R.E.; Kurylo, M.J. Photochemistry of Bromine-Containing Fluorinated Alkenes: Reactivity toward OH and UV Spectra. *J. Phys. Chem. A* **2002**, 106, 10195−10199.

(35) Banerjee, D.; Ghosh, A.; Chattopadhyay, S.; Ghosh, P.; Chaudhuri, R.K. Revisiting the 'cis-effect' in 1,2-Difluoro Derivatives of Ethylene and Diazene using *Ab Initio* Multireference Methods. *Mol. Phys.* **2014**, 112, 3206–3224.

(36) Jenkins, S.; Kirk, S.R.; Rong, C.; Yin, D. The Cis-effect Using the Topology of the Electronicc Charge Density. *Mol. Phys.* **2013**, 111, 793–805.

(37) Feller, D.; Peterson, K. A.; Dixon, D.A. Ab Initio Coupled Cluster Determination of the Heats of Formation of $C_2H_2F_2$, C_2F_2, and C_2F_4. *J. Phys. Chem. A* **2011**, 115, 1440–1451.

(38) Piccardo, M.; Penocchio, E.; Puzzarini, C.; Biczysko, M.; Barone, V. Semi-Experimental Equilibrium Structure determinations by Employing B3LYP/SNSD Anharmonic Force Fields: Validation and Application to Semirigid Organic Molecules. *J. Phys. Chem. A* **2015**, 119, 2058–2082.

(39) Feller, D.; Craig, N.C.; Groner, P.; McKean, D. C. *Ab Initio* Coupled Cluster Determination of the Equilibrium Structures of *cis*- and *trans*-1,2-Difluoroethylene and 1,1-Difluoroethylene. *J. Phys. Chem. A* **2011**, 115, 94–98.

(40) Krasnoshchekov, S. V.; Craig, N.C.; Stepanov, N.F. Anharmonic Vibrational Analysis of the Gas-Phase Infrared Spectrum of 1,1-Difluoroethylene Using the Operator Van Vleck Canonical Perturbation Theory. *J. Phys. Chem. A* **2013**, 117, 3041–3056.

(41) Nozirov, F.; Kupka, T.; Stachów, M. Theoretical prediction of nuclear magnetic shieldings and indirect spin-spin coupling constants in 1,1-, cis-, and trans-1,2-difluoroethylenes. *J. Chem. Phys.* **2014**, 140, 144303.

(42) Blanco, M.B.; Taccone, R.A.; Lane, S.I.; Teruel, M.A. Kinetics of the Reactions of $O(^3P)$ with $CCl_2=CH_2$, (Z)-CHCl=CHCl, and $CCl_2=CCl_2$: A Temperature Dependence Study. *J. Phys. Chem. A* **2006**, 110, 11091−11097.

(43) Scaranto, J.; Pietropolli Charmet, A.; Stoppa, P.; Giorgianni, S. Vinyl Halides on TiO_2 Surface: FTIR Spectroscopy Studies and Ab Initio Calculations. *J. Mol. Struct.* **2005**, 741, 213–219.

(44) Scaranto, J.; Stoppa, P.; Pietropolli Charmet, A.; Giorgianni, S. IR Spectroscopy of CH_2CBrF Adsorbed on TiO_2 and Quantum-Mechanical Studies. *Mol. Phys.* **2009**, 107, 237–244.

(45) Tasinato, N.; Moro, D.; Stoppa, P.; Pietropolli Charmet, A.; Toninello, P.; Giorgianni, S. Adsorption of $F_2C=CFCl$ on TiO2 Nano-Powder: Structures, Energetics and Vibrational Properties from DRIFT Spectroscopy and Periodic Quantum Chemical Calculations. *Appl. Surf. Sci.* **2015**, 353, 986–994.

(46) McKean, D.; Law, M.M.; Groner, P.; Conrad, A.R.; Tubergen, M.J.; Feller, D.; Moore, M.C.; Craig, N.C. Infrared Spectra of $CF_2=CHD$ and $CF_2=CD_2$: Scaled Quantum-Chemical Force Fields and an Equilibrium Structure for 1,1-Difluoroethylene. *J. Phys. Chem. A* **2010**, 114, 9309–9318.

(47) McKean, D. C.; van der Veken, B.; Herrebout, W.; Law, M. M.; Brenner, M. J.; Nemchick, D. J.; Craig, N. C. Infrared Spectra of $^{12}CF_2{}^{12}CH_2$ and $^{12}CF_2{}^{13}CH_2$, Quantum-Chemical Calculations of Anharmonicity, and Analyses of Resonances. *J. Phys. Chem. A* **2010**, 114, 5728−5742.

(48) Tasinato, N.; Pietropolli Charmet, A.; Stoppa, P.; Giorgianni, S.; Gambi, A. Quantum-Chemical *Ab Initio* Investigation of the Vibrational Spectrum of Halon 1113 and its Anharmonic Force Field: a Joint Experimental and Computational Approach. *Chem. Phys.* **2012**, 397, 55−64.

(49) Stoppa, P.; Pietropolli Charmet, A.; Giorgianni, S.; Ghersetti, S.; Gambi, A. Tunable Diode Laser Spectroscopy of cis-1,2-Difluoroethylene: Rovibrational Analysis of the ν_9 and $\nu_5+\nu_{10}$ Bands and Anharmonic Force Field. *J. Phys. Chem. A* **2003**, 107, 474−479.

(50) Stone, R.G.; Flygare, W.H. The Microwave Spectrum and ^{35}Cl Nuclear Quadrupole Coupling in Chlorotrifluoroethylene. *J. Mol. Spectrosc.* **1969**, 32, 233−241.

(51) Alonso, J.L.; Lesarri, A.G.;Leal, L.A.; Lòpez, J.C. The Millimeter-Wave Spectra of 1-Chloro-1-fluoroethylene and cis-1-Chloro-2-fluoroethylene. *J. Mol. Spectrosc.* **1993**, 162, 4−19.

(52) Vogelsanger, B.; Andrist, M.; Bauder, A. Two-Dimensional Correlation Experiments in Microwave Fourier Transform Spectroscopy. *Chem. Phys. Lett.* **1988**, 144, 180−186.

(53) Vogelsanger, B.; Bauder, A. Two-Dimensional Microwave Fourier Transform Spectroscopy. *J. Chem. Phys.* **1990**, 92, 4101−4114.

(54) Leung, H.O.; Marshall, M.D.; Vasta, A.L.; Craig, N.C. Microwave Spectra of Eight Isotopic Modifications of 1-Chloro-1-Fluoroethylene. *J. Mol. Spectrosc.* **2009**, 253, 116−121.

(55) Leung, H.O.; Marshall, M.D.; Bozzi, A.T.; Cohen, P.M.; Lam, M. Microwave Spectrum and Molecular Structure of the 1-Chloro-1-Fluoroethylene-Hydrogen Fluoride Complex. *J. Mol. Spectrosc.* **2011**, 267, 43−49.

(56) Locht, R.; Dehareng, D.; Leyh, B. Vibronic Valence and Rydberg Transitions in Geminal Chloro-Fluoro-Ethene (1,1-C_2H_2FCl): a Spectroscopic and Quantum Chemical Investigation. *Mol. Phys.* **2014**, 112, 1520−1539.

(57) Locht, R.; Dehareng, D.; Leyh, B. The Threshold Photoelectron Spectrum of the Geminal Chloro-Fluoro-Ethene (1,1-C_2H_2FCl) Isomer. Experiment and Theory. *J. Phys. B: At., Mol. Opt. Phys.* **2014**, 47, 085101.

(58) Scott, J.D.; Russel, B.R. Vacuum-Ultraviolet Spectral Studies of Several Chlorofluoroethylenes. *J. Am. Chem. Soc.* **1972**, 94, 2634−2638.

(59) Huang, C.-H.; Chou, S.Y.; Jang, S.-B.; Lin, Y.-C.; Li, C.-E.; Chen, C.-C.; Chang, J.-L. Insights into the Photoelectron Spectroscopy of Chlorofluoroethenes Studied by Density-Functional and Coupled-Cluster Theories *J. Phys. Chem. A* **2016**, 120, 1175−1183.

(60) Pietropolli Charmet, A.; Stoppa, P.; Giorgianni, S.; Ghersetti, S. The Infrared Laser Spectrum of CH_2=CFCl near 1190 cm^{-1}; Rovibrational Analysis of the C-F Stretching Mode. *J. Mol. Struct.* **2001**, 599, 31−38.

(61) Pietropolli Charmet, A.; Stoppa, P.; Visinoni, R.; Giorgianni, S.; Nivellini, G.D. High-Resolution FTIR Spectra of CH_2=CFCl in the 930-1050 cm^{-1} Region. *Mol. Phys.* **2002**, 100, 3529−3534.

(62) Scaranto, J.; Pietropolli Charmet, A.; Giorgianni, S. IR Spectroscopy and Quantum-Mechanical Studies of the Adsorption of CH_2CClF on TiO_2. *J. Phys. Chem. C* **2008**, 112, 9443−9447.

(63) Torkington P.; Thompson, H.W. The Infra-Red Spectra of Fluorinated Hydrocarbons *Trans. Faraday Soc.* **1945**, 41, 236–245.

(64) Mann, D.E.; Acquista, N.; Plyler, E.K. Vibrational Spectrum of 1-Fluoro-1-Chloroethylene. *J. Chem. Phys.* **1955**, 23, 2122−2126.

(65) Nielsen, J.R.; Albright, J.C. Raman Spectrum of Gaseous 1-Fluoro-1-Chloroethylene. *J. Chem. Phys.* **1957**, 26, 1566–1567.

(66) Purvis, G. D.; Bartlett, R. J. A Full Coupled-Cluster Singles and Doubles Model: the Inclusion of Disconnected Triples. *J. Chem. Phys.* 1982, **76**, 1910−1918.

(67) Raghavachari, K.; Trucks, G. W.; Pople, J. A.; Head-Gordon, M. A Fifth-Order Perturbation of Electron Correlation Theories. *Chem. Phys. Lett.* **1989**, 157, 479–483.

(68) Hampel, C.; Peterson, K.A.; Werner, H.-J. A Comparison of the Efficiency and Accuracy of the Quadratic Configuration Interaction (QCISD), Coupled Cluster (CCSD), and Brueckner Coupled Cluster (BCCD) Methods. *Chem. Phys. Lett.* **1992**, 190, 1–12.

(69) Møller, C.; Plesset, M. S. Note on an Approximation Treatment for Many-Electron Systems. *Phys. Rev.* **1934**, 46, 618−622.

(70) Grimme, S. Semiempirical Hybrid Density Functional with Perturbative Second-Order Correlation. *J. Chem. Phys.* **2006**, 124, 034108.

(71) Biczysko, M.; Panek, P.; Scalmani, G.; Bloino, J.; Barone, V. Harmonic and Anharmonic Vibrational Frequency Calculations with the Double-Hybrid B2PLYP Method: Analytic Second Derivatives and Benchmark Studies. *J. Chem. Theory Comput.* **2010**, 6, 2115−2125.

(72) Krasnoshchekov, S. V.; Craig, N. C.; Boopalachandran, P.; Laane, J.; Stepanov, N. F. Anharmonic Vibrational Analysis of the Infrared and Raman Gas-Phase Spectra of s-trans- and s-gauche-1,3-Butadiene. *J. Phys. Chem. A* **2015**, 119, 10706 – 10723.

(73) Ahro, M.; Kauppinen, J. Nonlinearity of Beer's Law in Gas-Phase FT-IR Spectroscopy. *Appl. Spectrosc.* **2001** 55, 50−54.

(74) Parker, F. ; Tooke, P. B. The Effect of Apodisation and Finite Resolution on Fourier Transform Infrared and Raman Spectra. *Spectrochim. Acta A* **1997**, 53, 2245−2252.

(75) Pietropolli Charmet, A.; Tasinato, N.; Stoppa, P.; Baldacci, A.; Giorgianni, S. Jet-Cooled Diode Laser Spectrum and FTIR Integrated Band Intensities of CF_3Br: Rovibrational Analysis of $2\nu_5$ and $\nu_2+\nu_3$ Bands Near 9 μm and Cross-Section Measurements in the 450–2500 cm^{-1} Region. *Mol. Phys.* **2008**, 106, 1171−1179.

(76) Pietropolli Charmet, A.; Stoppa, P.; Tasinato, N.; Baldan, A.; Giorgianni, S.; Gambi, A. Spectroscopic Study of $CHBrF_2$ up to 9500 cm^{-1}: Vibrational Analysis, Integrated Band Intensities, and *Ab Initio* Calculations. *J. Chem. Phys.* **2010**, 133, 044310.

(77) Schneider, W.; Thiel, W. Anharmonic Force Fields from Analytic Second Derivatives: Method and Application to Methyl Bromide. *Chem. Phys. Lett.* **1989**, 157, 367–373.

(78) *In preparation.*

(79) Dunning Jr., T.H. Gaussian Basis Sets for Use in Correlated Molecular Calculations. I. The Atoms Boron through Neon and Hydrogen. *J. Chem. Phys.* **1989**, 90, 1007−1023.

(80) Woon, D.E.; Dunning Jr, T.H. Gaussian Basis Sets for Use in Correlated Molecular Calculations. III. The Atoms Aluminum through Argon. *J. Chem. Phys.* **1993**, 98, 1358−1371.

(81) Kendall, R.A.; Dunning Jr, T.H.; Harrison, R.J. Electron Affinities of the First-Row Atoms Revisited. Systematic Basis Sets and Wave Functions. *J. Chem. Phys.* **1992**, 96, 6796−6806.

(82) Carnimeo, I.; Puzzarini, C.; Tasinato, N.; Stoppa, P.; Pietropolli Charmet, A.; Biczysko, M.; Cappelli, C.; Barone, V. Anharmonic Theoretical Simulations of Infrared Spectra of Halogenated Organic Compounds. *J. Chem. Phys.* **2013**, 139, 074310.

(83) Woon, D.E.; Dunning Jr, T.H. Gaussian Basis Sets for Use in Correlated Molecular Calculations. V. Core-Valence Basis Sets for Boron through Neon. *J. Chem. Phys.* **1995**, 103, 4572−4585.

(84) Peterson, K.A.; Dunning Jr, T.H. Accurate Correlation Consistent Basis Sets for Molecular Core-Valence Correlation Effects: the Second Row Atoms Al-Ar, and the First Row Atoms B-Ne Revisited. *J. Chem. Phys.* **2002**, 117, 10548−10560.

(85) Almlöf, J.; Taylor, P.R. General Contraction of Gaussian Basis Sets. I. Atomic Natural Orbitals for First- and Second Row Atoms. *J. Chem. Phys.* **1987**, 86, 4070−4077.

(86) Widmark, P.-O.; Persson, B.J.; Roos, B.O. Density Matrix Averaged Atomic Natural Orbital (ANO) Basis Sets for Correlated Molecular Wave Functions. *Theor. Chim. Acta* **1991**, 79, 419–432.

(87) CFOUR, Coupled-Cluster techniques for Computational Chemistry, a quantum-chemical program package by Stanton, J.F.; Gauss, J. ; Harding, M.E. *et al.*, and the integral packages MOLECULE (Almlöf, J.; Taylor, P.R.), PROPS (Taylor, P.R.), ABACUS (Helgaker, T.; Jensen, H.J. Aa. ; Jørgensen, P. and Olsen, J.), and ECP routines by Mitin, A. V., and Wüllen, C. For the current version, see http://www.cfour.de.

(88) Frisch, M. J.; Trucks, G. W. ; Schlegel, H. B. et al., Gaussian 09, Revision D.01, Gaussian, Inc., Wallingford, CT, 2009.

(89) Nielsen, H.H. The Vibration-Rotation Energies of Molecules. *Rev. Mod. Phys.* **1951** 23, 90–136.

(90) Amat, G.; Nielsen, H.H.; Tarrago, G. *Rotation-Vibration of Polyatomic Molecules*: New York: Marcel Decker: Amsterdam, 1971.

(91) Papoušek, D.; Aliev, M. R.; *Molecular Vibrational-Rotational Spectra*; Elsevier: Amsterdam, 1982.

(92) Martin, J. M. L.; Lee, T. J.; Taylor, P. M.; François, J.-P. The Anharmonic Force Field of Ethylene, C_2H_4, by Means of Accurate Ab Initio Calculations. *J. Chem. Phys.* **1995**, 103, 2589–2602.

(93) Darling, B.; Dennison, D. The Water Vapor Molecule. *Phys. Rev.* **1940**, 57, 128–139.

(94) Piccardo, M; Bloino, J.; Barone, V. Generalized Vibrational Perturbation Theory for Rotovibrational Energies of Linear, Symmetric and Asymmetric Tops: Theory, Approximations, and Automated Approaches to Deal with Medium-to-Large Molecular Systems. *Int. J. Quantum Chem.* **2015**, 115, 948–982, and references therein.

(95) Martin, J. M. L.; Taylor, P. R. Accurate ab initio quartic force field for trans-HNNH and treatment of resonance polyads. *Spectrochim. Acta, Part A*, **1997**, 53, 1039– 1050.

(96) Rosnik, A. M.; Polik, W. F. VPT2+K Spectroscopic Constants and Matrix Elements of the Transformed Vibrational Hamiltonian of a Polyatomic Molecule with Resonances using Van Vleck Perturbation Theory. *Mol. Phys.* **2014**, 112, 261–300.

(97) Gaw, J. F. ; Willets, A.; Green, W. H.; Handy, N. C. *Advances in Molecular Vibrations and Collision Dynamics*; edited by J. M. Bowman, JAI Press: Greenwich, 1990, p. 169, SPECTRO.

(98) Borro, A. F. ; Mills, I. M.; Venuti, E. Quartic Anharmonic Resonances in Acetylenes and Haloacetylenes. *J. Chem. Phys.* **1995**, 102, 3938–3944.

(99) Tasinato, N.; Regini, G.; Stoppa, P.; Pietropolli Charmet, A.; Gambi, A. Anharmonic Force Field and Vibrational Dynamics of CH_2F_2 up to 5000 cm^{-1} Studied by Fourier Transform Infrared Spectroscopy and State-of-the-Art *Ab Initio* Calculations. *J. Chem. Phys.* **2012**, 136, 214302.

(100) Bloino, J.; Biczysko, M.; Barone, V. General Perturbative Approach for Spectroscopy, Thermodynamics, and Kinetics: Methodological Background and Benchmark Studies. *J. Chem. Theory Comput.* **2012**, 8, 1015–1036.

(101) Kuhler, K. M.; Truhlar, D. G.; Isaacson, A. D. General Method for Removing Resonance Singularities in Quantum Mechanical Perturbation Theory. *J. Chem. Phys.* **1996**, 104, 4664 – 4670.

(102) Pietropolli Charmet, A.; Stoppa, P.; Tasinato, N.; Giorgianni, S.; Barone, V.; Biczysko, M.; Bloino, J.; Cappelli, C.; Carnimeo, I.; Puzzarini, C. An Integrated Experimental and Quantum-Chemical Investigation on the Vibrational Spectra of Chlorofluoromethane. *J. Chem. Phys.* **2013**, 139, 164302.

(103) Martin, J.M.L.; Taylor, P.R. Basis Set Convergence for Geometry and Harmonic Frequencies. Are h Functions Enough? *Chem. Phys. Lett.* **1994**, 225, 473–479.

(104) Wang, X.-G.; Sibert III, E.L.; Martin, J.M.L. Anharmonic Force Field and Vibrational Frequencies of Tetrafluoromethane (CF_4) and Tetrafluorosilane (SiF_4). *J. Chem. Phys.* **2000**, 112, 1353−1366.

(105) Allen, W. D.; Császár, A. G.; Horner, D. A.; The Puckering Inversion Barrier and Vibrational Spectrum of Cyclopentene. A Scaled Quantum Mechanical Force Field Algorithm. *J. Am. Chem. Soc.* **1992**, 114, 6834–6849.

(106) Smith, D.C.; Nielsen, J.R.; Claassen, H.H. Infra-Red and Raman Spectra of Fluorinated Ethylenes. I. 1,1-Difluoroethylene. *J. Chem. Phys.* **1950**, 18, 326–331.

(107) Krasnoshchekov, S. V.; Isayeva, E. V.; Stepanov, N. F. Criteria for first- and second-order vibrational resonances and correct evaluation of the Darling-Dennison resonance coefficients using the canonical Van Vleck perturbation theory. *J. Chem. Phys.* **2014**, 141, 234114.

(108) Stoppa, P.; Pietropolli Charmet, A.; Tasinato, N.; Giorgianni, S.; Gambi, A. Infrared Spectra, Integrated Band Intensities, and Anharmonic Force Field of H_2C=CHF. *J. Phys. Chem. A* **2009**, 113, 1497–1504.

(109) Mills, I. M.; Robiette, G. On the Relationship of Normal Modes to Local Modes in Molecular Vibrations. *Mol. Phys.* **1985**, 56, 743–765.

(110) Pyykkö, P. The Nuclear Quadrupole Moments of the 20 First Elements: High-Precision Calculations on Atoms and Small Molecules. *Z. Naturforsch.* **1992**, 47a , 189–196.

(111) Chu, P. M.; Guenther, F. R.; Rhoderick, G. C.; Lafferty, W. J. The NIST Quantitative Infrared Database. *J. Res. Natl. Inst. Stand. Technol.* **1999**, 104, 59–81.

Figure Captions

Figure 1. Molecular structure of $ClFC=CH_2$ and its principal axes of inertia: the *a* and *b* axes are in the molecular plane, the *c* axis is perpendicular to it.

Figure 2. Survey spectra of $ClFC=CH_2$ in the region 400 – 6400 cm^{-1} (resolution = 1.0 cm^{-1}, optical path length = 13.4 cm, room temperature). Trace ***a*** refers to the spectrum recorded employing a sample pressure of 376 Pa, trace ***b*** (displaced for clarity) to the one obtained with a sample pressure of 61.28 hPa. Only some representative bands are labeled.

Figure 3. Spectra of $ClFC=CH_2$ in the 460 – 760 cm^{-1} region (resolution = 0.5 cm^{-1}, optical path length = 13.4 cm , room temperature). Trace ***a*** refers to the spectrum measured employing a sample pressure of 800 Pa, trace ***b*** to the one obtained at 400 hPa, trace ***c*** to that one recorded at 660 hPa. Only ν_7 and ν_{12} bands are labeled.

Figure 4. Spectrum of $ClFC=CH_2$ in the 2900 – 3200 cm^{-1} region (resolution = 0.2 cm^{-1}, optical path length = 13.4 cm , room temperature, sample pressure = 400 hPa).

Figure 5. Spectrum of $ClFC=CH_2$ in the 5900 – 6400 cm^{-1} region (resolution = 0.2 cm^{-1}, optical path length = 13.4 cm , room temperature, sample pressure = 120.2 hPa). The absorptions assigned to the triad $2\nu_1/\nu_1+\nu_2/2\nu_2$ are labeled.

Figure 6. Absorption cross section spectra of $ClFC=CH_2$ (T = 298 K, resolution = 0.5 cm^{-1}). The most important absorptions are labeled.

Table 1. Equilibrium geometries and rotational constants of $^{35}ClFC=CH_2$ obtained at CCSD(T) level of theory and employing different basis sets[a]

	VTZ[b]	VTZ-AVTZ(F)[b]	CVTZ-ACVTZ(F)[b]	ANO2[b]
C_2–F_1	1.3304	1.3559	1.3344	1.3321
C_2=C_3	1.3286	1.3282	1.3252	1.3279
C_3–H_4	1.0800	1.0801	1.0790	1.0802
C_2–Cl_5	1.7245	1.7218	1.7140	1.7194
C_3–H_6	1.0775	1.0777	1.0767	1.0778
< C_3–C_2–F_1	122.7	122.4	122.3	122.6
< C_3–C_2–Cl_5	125.2	125.8	125.9	125.5
< C_2–C_3–H_6	120.2	120.1	120.1	120.1
< C_2–C_3–H_4	119.3	119.3	119.4	119.4
A_e	10654.86681	10648.19902	10691.88168	10653.40565
B_e	5052.52871	5050.61532	5084.90533	5072.94900
C_e	3427.30406	3425.73368	3446.02524	3436.53598

[a] Bond lengths and angles reported in Å and deg, respectively; equilibrium rotational constants listed in MHz. See text for labeling of the atoms.

[b] VTZ stands for cc-pVTZ basis set on all atoms; VTZ-AVTZ(F) stands for cc-pVTZ basis set on C, H and Cl atoms and aug-cc-pVTZ on F atom; CVTZ-ACVTZ stands for calculation carried out with all the electrons correlated and employing the cc-pCVTZ basis set on C, H and Cl atoms and the aug-cc-pCVTZ basis set on F atom.

Table 2. Harmonic wavenumbers (*Wvn*) and intensities (*I*) of $^{35}ClFC=CH_2$ calculated at CCSD(T) level of theory and using different basis sets

		VTZ[a]		VTZ-AVTZ(F)[a]		CVTZ-ACVTZ(F)[a]		ANO2[a]	
Mode	Sym.[b]	*Wvn*[c]	*I*[c]	*Wvn*[c]	*I*[c]	*Wvn*[c]	*I*[c]	*Wvn*[c]	*I*[c]
ω_1	A'	3300.8	0.19	3299.3	0.21	3304.8	0.23	3301.2	0.25
ω_2	A'	3193.3	2.74	3191.5	3.05	3195.4	3.11	3193.3	3.09
ω_3	A'	1706.5	129.57	1704.2	125.53	1708.5	125.37	1702.8	120.8
ω_4	A'	1413.6	3.77	1410.3	2.78	1412.4	2.49	1406.8	2.13
ω_5	A'	1221.1	173.75	1207.9	176.7	1210.4	175.98	1213.0	166.88
ω_6	A'	967.4	34.72	960.5	40.06	962.1	39.91	963.9	35.86
ω_7	A'	701.5	39.58	702.07	37.48	706.1	36.93	702.3	37.96
ω_8	A'	432.7	1.58	429.7	1.85	432.2	1.86	432.4	1.74
ω_9	A'	368.8	0.07	366.4	0.08	368.9	0.07	369.7	0.02
ω_{10}	A"	849.1	55.87	848.8	54.68	851.4	54.84	847.9	53.49
ω_{11}	A"	723.6	0.20	722.6	0.06	724.2	0.06	722.2	0.24
ω_{12}	A"	523.1	0.58	519.7	0.68	523.4	0.78	520.4	1.07

[a] VTZ stands for cc-pVTZ basis set on all atoms; VTZ-AVTZ(F) stands for cc-pVTZ basis set on C, H and Cl atoms and aug-cc-pVTZ on F atom; CVTZ-ACVTZ stands for cc-pCVTZ basis set on C, H and Cl atoms and the aug-cc-pCVTZ basis set on F atom (all electron correlated).
[b] Symmetry.
[c] Wavenumber (*Wvn*) and intensity (*I*) reported in cm^{-1} and km mol^{-1}, respectively.

Table 3. Definition of symmetry adapted internal coordinates of ClFC=CH$_2$ in terms of internal coordinates

Symmetry Species	Symmetry coordinates	Internal coordinates[a]
A'	S_1	$\frac{1}{\sqrt{2}}(r_{34} + r_{36})$
	S_2	r_{23}
	S_3	r_{12}
	S_4	r_{25}
	S_5	$\frac{1}{\sqrt{2}}(\alpha_{234} + \alpha_{236})$
	S_6	$\frac{1}{\sqrt{2}}(r_{34} - r_{36})$
	S_7	$\frac{1}{\sqrt{2}}(\alpha_{234} - \alpha_{236})$
	S_8	α_{123}
	S_9	α_{325}
A"	S_{10}	$\frac{1}{\sqrt{2}}(\gamma_{4326} + \gamma_{6342})$
	S_{11}	$\frac{1}{\sqrt{2}}(\gamma_{1235} + \gamma_{5213})$
	S_{12}	$\frac{1}{\sqrt{2}}(\tau_{1234} + \tau_{5236})$

[a] See text for labeling.

Table 4. Approximate description, Total Energy Distribution (TED%) in terms of symmetry-adapted internal coordinates of ClFC=CH_2 as computed at CCSD(T)/CVTZ-ACVTZ(F) level of theory, and the corresponding wavenumbers (*Wvn*, in cm^{-1})

Approximate description	Mode	TED	*Wvn*
anti-sym. CH_2 stretch.	ω_1	S_6(99)	3304.8
symm. CH_2 stretch.	ω_2	S_1(98)	3195.4
C=C stretch.	ω_3	S_2(76)	1708.5
CH_2 scissors	ω_4	S_5(87)	1412.4
C-F stretch.	ω_5	S_3(41) + S_7(31)	1210.4
CH_2 rock	ω_6	S_7(50) + S_3(42)	962.1
C-Cl stretch.	ω_7	S_4(67) + S_8(12)	706.1
C=C-F bending	ω_8	S_8(83) + S_4(18)	432.2
C=C-Cl bending	ω_9	S_9(104)	368.9
CH_2 wag	ω_{10}	S_{10}(100)	851.4
torsion	ω_{11}	S_{12}(94)	724.2
C=CClF out-of-plane	ω_{12}	S_{11}(94)	523.4

TABLE 5. Summary of the assigned bands (cm^{-1}) from the gas-phase infrared spectra of $ClFC=CH_2$

Band	Wavenumber[a]	Band	Wavenumber[a]	Band	Wavenumber[a]	Band	Wavenumber[a]
ν_8	432.2(2)/428.3(2)[b]	$\nu_6+\nu_9$	1317.5(4)/1315.7(4)[b]	$\nu_3+2\nu_8$	2523.5(5)	$\nu_2+\nu_5$	4253.9(3)
$\nu_8+\nu_9-\nu_9$	432.9(3)	$\nu_{10}+\nu_{12}$	1338.1(3)	$\nu_5+\nu_6+\nu_8$	2540.3(5)	$\nu_1+\nu_7+\nu_8$	4283.5(5)
ν_{12}	514.7(2)/514.2(2)[b]	ν_4	1374.7(2)	$\nu_4+\nu_5$	2559.8(5)	$\nu_1+\nu_5$	4343.5(3)
ν_7	700.3(3)	$\nu_7+\nu_{11}$	1407.6(4)/1405.7(4)[b]	$\nu_3+\nu_6$	2602.9(5)	$\nu_3+2\nu_4$	4398.8(5)
$2\nu_9$	741.7(3)/737.9(3)[b]	$\nu_6+\nu_{12}$	1460.5(5)	$\nu_3+2\nu_{12}$	2687.4(5)	$\nu_1+\nu_4$	4516.5(3)
$3\nu_9-\nu_9$	743.4(3)	$\nu_{10}+\nu_{11}$	1537.1(4)	$2\nu_4$	2741.7(5)	$\nu_1+2\nu_7$	4563.4(3)
$\nu_7+\nu_8-\nu_9$	756.3(3)	$\nu_5+\nu_9$	1556.9(4)	$\nu_3+\nu_5$	2840.3(4)	$\nu_1+\nu_5+\nu_8$	4754.6(5)
ν_{10}	835.5(2)	ν_3	1655.8(2)	$\nu_3+\nu_6+\nu_9$	2968(1)	$\nu_1+\nu_6+\nu_7$	4793.1(5)
$\nu_{10}+\nu_9-\nu_9$	836.9(3)	$2\nu_{10}$	1689.6(3)	$\nu_3+\nu_4$	3020.2(5)	$\nu_1+\nu_3$	4834.9(3)
$2\nu_8$	860.3(3)/854.2(3)[b]	$\nu_6+\nu_{10}$	1784.9(4)	ν_2	3072.1(3)	$\nu_2+\nu_5+\nu_7$	4923.2(5)
$\nu_9+\nu_{12}$	896.2(3)	$2\nu_6$	1893.9(4)	ν_1	3158.9(5)	$3\nu_3$	4969.7(5)
$\nu_8+\nu_{10}-\nu_9$	899.6(3)	$\nu_3+\nu_9$	2024.9(4)	$2\nu_5+\nu_6$	3285.1(3)	$\nu_2+\nu_3+\nu_6$	5661(1)
ν_6	947.7(2)	$\nu_4+\nu_7$	2060.3(4)	$2\nu_3$	3325.9(3)	$\nu_1+\nu_4+\nu_5$	5699(1)
$\nu_4-\nu_9$	1004.2(3)	$\nu_5+\nu_6$	2130.2(3)	$\nu_3+\nu_4+\nu_9$	3397.7(3)	$2\nu_2$	6042.6(3)
$2\nu_{12}$	1027.8(3)/1026.9(3)[b]	$\nu_3+\nu_{12}$	2184.5(3)	$\nu_1+\nu_9$	3529.2(5)	$\nu_1+\nu_2$	6106.2(3)
$\nu_7+\nu_9$	1063.2(3)	$2\nu_5$	2370.4(4)	$\nu_2+\nu_{10}$	3899.1(5)	$\nu_1+\nu_3+\nu_4$	6166.5(5)
$\nu_9+\nu_{11}$	1075.9(5)	$\nu_5+\nu_8+\nu_{10}$	2451.2(5)	$\nu_1+\nu_{10}$	3978.2(5)	$2\nu_1$	6272.6(3)
ν_5	1188.1(3)	$\nu_6+\nu_7+\nu_{10}$	2471.3(5)	$\nu_2+\nu_6$	4010.9(5)		
$\nu_{11}+\nu_{12}$	1221.8(3)	$\nu_3+\nu_{10}$	2486.6(5)	$\nu_1+\nu_6$	4101.2(3)		

[a] The experimental error in parentheses is on the last significant digit.

[b] $^{35/37}Cl$ isotopologues.

TABLE 6. The observed and calculated (at CCSD(T) level of theory employing the CVTZ-ACVTZ(F) basis set) gas-phase infrared frequency fundamentals (cm^{-1}) of $^{35}ClFC=CH_2$

			GVPT2[a]		HDCPT2[b]	
Band	Symmetry	Observed[c]	Calculated[c,d]	Obs. – Calc.[c]	Calculated[c]	Obs. – Calc.[c]
ν_1	A'	3158.9(5)	3159.6	–0.7	3161.8	–2.9
ν_2	A'	3072.1(2)	3071.6*	–0.5	3072.4	–0.3
ν_3	A'	1655.8(2)	1653.6*	2.2	1681.6	–25.8
ν_4	A'	1374.7(2)	1376.8*	–2.1	1374.4	0.3
ν_5	A'	1188.1(2)	1184.5	3.6	1184.0	4.1
ν_6	A'	947.7(2)	944.7	3.0	944.0	3.7
ν_7	A'	700.3(3)	696.7	3.6	694.8	5.5
ν_8	A'	432.2(2)	429.8	2.4	429.7	2.5
ν_9	A'	370[e]	368.0	2.0	367.7	2.3
ν_{10}	A"	835.5(2)	834.6	0.9	823.9	11.6
ν_{11}	A"	—[f]	708.7	—	708.7	—
ν_{12}	A"	514.7(2)	515.5	–0.8	515.8	–1.1

[a] Generalized second-order Vibrational Perturbational Theory, see Ref. 94.
[b] Hybrid Degeneracy-Corrected second-order Perturbation Theory, see Ref. 100.
[c] All the values in cm^{-1}.
[d] Values marked by an asterisk are computed taking into account anharmonic resonances (see discussion in the text).
[e] Value taken from Ref. 65.
[f] Covered by the stronger absorption of ν_7 centered at 700.3(3) cm^{-1}.

TABLE 7. Anharmonicity constants $x_{i,j}$ (cm^{-1}) of $^{35}ClFC=CH_2$[a]

i/j	1	2	3	4	5	6	7	8	9	10	11	12
1	–32.7 [–22.6 ±0.3]											
2	–105.4 [–124.8±0.5]	–28.4 [–50.8±0.3]										
3	1.0 [20.2±0.5]	–11.5* (+2.03)	–6.0 [7.2±0.3; –6.4±0.4][b]									
4	–21.2 [–16.6±0.5]	–16.7* (–3.19)	–4.6* (–18.1) [–9.8±0.6]	–4.3 [-3.4±0.3]								
5	–3.8 [–3.5±0.5]	–4.5 [–6.3±0.5]	–8.8 [–3.6±0.6]	–3.7 [–2.5±0.6]	–3.1 [–2.9±0.4]							
6	–5.6 [–5.4±0.5]	–4.6 [–8.9±0.6]	–6.8 [–0.6±0.6]	–3.6	–6.3 [–5.6±0.5]	–0.9 [–0.8±0.3]						
7	–0.7	–1.0	0.0	–0.7*(62.0) [–14.2±0.5]	–3.6	–3.3	–1.0* (–16.7)					
8	–0.4	–0.2	–1.8	0.5	–2.2	–1.4	–1.8	0.2 [–2.1±0.3]				
9	–0.3	–0.4	–2.1	0.4	–1.7 [–1.2±0.5]	–0.1	–1.5	1.0	0.5 [1.2±0.3]			
10	–16.5 [–16.2±0.6]	–9.7 [–8.5±0.6]	–8.7* (+112.4) [–4.7±0.6]	–10.8*(0.3)	0.4	2.2 [1.7±0.5]	0.1	0.7	0.7	2.8* (–27.4) [9.3±0.3]		
11	–5.9	–6.7	–3.8	–2.0* (–23.5)	–2.8	–0.2	–0.5	–0.1	–0.1	–5.2	–0.8* (4.6)	
12	–0.9	–1.1	–5.4 [14.0±0.5]	–1.0* (9.5)	–2.2	–1.7 [–1.9±0.6]	–1.9	0.1	0.2	2.2* (0.2) [–12.1±0.4]	–0.7	–0.8 [–0.8±0.3]

[a] *Ab initio* deperturbed constants are marked by an asterisk (in parentheses are reported the values altered by nearly singular terms, see text); experimental values, together with the corresponding errors, are listed within square brackets.

[b] The first value is computed from the position of $2\nu_3$ and ν_3 bands, the second one from $3\nu_3$ and $2\nu_3$ bands. The difference is due to Fermi resonance involving ν_3 and $2\nu_{10}$ (see text).

TABLE 8. Anharmonic vibration-rotation α constants for ClFC=CH$_2$ computed at CCSD(T)/CVTZ-ACVTZ(F) level of theory[a]

		^{35}ClFC=CH$_2$			^{37}ClFC=CH$_2$		
Symmetry	Mode	α_A	α_B	α_C	α_A	α_B	α_C
A'	1	13.350	1.546	1.870	13.354	1.471	1.803
	2	7.621	2.885	2.137	7.624	2.763	2.074
	3	39.894	10.760	8.991	39.920	10.404	8.764
	4	–10.342	0.045	1.236	-10.347	0.098	1.214
	5	31.392 (32.7169)[b]	8.826 (12.42295)[b]	12.330 (11.71796)[b]	31.376	8.607	11.980
	6	9.413 (9.94562)[c]	–4.596 (–4.28808)[c]	2.951 (3.05437)[c]	9.462	–4.318	2.848
	7	0.649[d]	25.856	10.014	0.377[d]	23.073	9.760
	8	0.630	–0.863	–7.962	0.718	–0.826	–7.904
	9	–11.593	–1.539	13.387	–11.846	–1.443	13.216
A"	10	20.054	2.676	–1.927	20.255	2.451	–1.870
	11	20.548[d]	–6.889	–0.303	16.941[d]	–4.865	–0.598
	12	–8.406 (–9.48018)[c]	2.188 (1.98710)[c]	–3.018 (–3.02756)[c]	–8.795 (–8.96558)[c]	2.248	–2.987

[a] All values in MHz.
[b] Experimental values taken from Ref. 60.
[c] Experimental values taken from Ref. 61.
[d] Values deperturbed by the effect due to Coriolis resonance (see text).

TABLE 9. Spectroscopic parameters of ClFC=CH_2 relevant to rotational spectroscopy

	^{35}Cl		^{37}Cl	
	Experimental[a]	Computed[b]	Experimental[a]	Computed[b]
A_0 /MHz	10681.65141(47)	10635.277	10681.32209(40)	10637.074
B_0 /MHz	5102.15417(16)	5064.458	4955.24868(17)	4918.577
C_0 /MHz	3448.30884(18)	3426.172	3380.51600(20)	3358.934
Δ_J /kHz	1.4231(86)	1.39090	1.3323(69)	1.31891
Δ_{JK} /kHz	4.987(32)	5.04291	4.861(54)	4.90144
Δ_K /kHz	5.157(80)	4.99625	5.277(80)	5.20362
δ_J /kHz	0.4832(30)	0.47648	0.4503(26)	0.44571
δ_K /kHz	5.434(35)	5.36951	5.268(66)	5.22362
Φ_J /Hz	0.00107(8)	0.00085	0.00051(7)	0.000772
Φ_{JK} /Hz	0.0133(9)	0.01465	0.0181(9)	0.01384
Φ_{KJ} /Hz	–0.011(2)	–0.01407	–0.023(2)	–0.0128
Φ_K /Hz	0.024(1)	0.02576	0.032(2)	0.0252
ϕ_J /Hz	0.00036(5)	0.00044	0.00057(4)	0.000403
ϕ_{JK} /Hz	0.010(1)	0.00891	0.004(1)	0.0084
ϕ_K /Hz	0.092(3)	0.09498	0.108(4)	0.0944
χ_{aa} /MHz	–72.9696(13)	–72.12808	–57.49659(95)	–56.83385
χ_{bb} /MHz	38.6765(13)	38.00352	30.4711(11)	29.93960
χ_{cc} /MHz	34.2932(14)	34.12456	27.0255(11)	26.89424
χ_{ab} /MHz		6.44245		5.17676

[a] Experimental ground state rotational constants (MHz) and quartic centrifugal distortion constants (kHz) taken from Ref. 54, while sextic distortion terms (Hz) taken from Ref. 51. Experimental quadrupole coupling constants (MHz) are taken from Ref. 54.

[b] Values computed at CCSD(T) level of theory and employing the CVTZ-ACVTZ(F) basis set.

TABLE 10. Integrated cross sections (km mol^{-1}) in the range 400 – 6400 cm^{-1} for ClFC=CH$_2$

Integration limits (cm^{-1})	Main bands	Experimental[a]	HYB-MP2-1[b]	HYB-B2PLYP-1[b]	HYB-MP2-2[b]	HYB-B2PLYP-2[b]
400 – 455	ν_8	1.63(11)	1.74	1.74	1.62	1.62
500 – 520	ν_{12}	0.94(4)	0.79	0.73	1.08	1.02
650 – 750	ν_7, $2\nu_9$	39.3(2)	37.68	37.77	38.59	38.80
780 – 900	ν_{10}, $2\nu_8$, $\nu_9+\nu_{12}$	50.6(5)	52.77	53.14	51.32	51.79
900 – 1000	ν_6	41.9(2)	40.67	40.91	36.58	36.86
1000 – 1060	$2\nu_{12}$	2.60(2)	2.20	2.21	2.13	2.21
1090 – 1260	ν_5, $\nu_{11} + \nu_{12}$	166.2(5)	167.8	168.4	159.0	159.3
1260 – 1440	ν_4, $\nu_{10} + \nu_{12}$, $2\nu_{11}$	5.27(5)	2.42	2.50	2.04	2.14
1490 – 1580	$\nu_{10} + \nu_{11}$, $\nu_5 + \nu_9$	1.59(6)	1.32	1.18	1.38	1.18
1580 – 1790	ν_3 , $2\nu_{10}$, $\nu_6 + \nu_7$	130(3)	128	130	126	125
1840 – 1950	$2\nu_6$	2.42(2)	2.02	2.54	2.02	2.54
1950 – 2180	$\nu_5 + \nu_6$	1.87(3)	1.39	1.44	1.39	1.44
2180 – 200	$\nu_3 + \nu_{12}$	0.024(2)	0.04	0.05	0.04	0.05
2270 – 2420	$2\nu_5$	1.42(13)	0.94	0.79	0.94	0.79
2420 – 2920	$\nu_3 +\nu_{10}$, $\nu_4 + \nu_5$, $\nu_3 + \nu_6$, $\nu_3 + \nu_5$	2.51(7)	2.13	2.15	2.13	2.15
2920 – 3190	ν_1 , ν_2	1.87(3)	0.83	1.41	0.79	1.41
3200 – 3480	$2\nu_3$	1.69(5)	1.88	1.46	1.88	1.46
3950 – 4050	$\nu_2 + \nu_6$	0.198(7)	0.20	0.16	0.20	0.16
4050 - 4150	$\nu_1 + \nu_6$	0.345(3)	0.38	0.33	0.38	0.33
4150 – 4305	$\nu_2 + \nu_5$	0.629(5)	0.65	0.71	0.65	0.71
4305 – 4420	$\nu_1 + \nu_5$	0.487(3)	0.44	0.51	0.44	0.51
4420 – 4600	$\nu_1 + \nu_4$	1.056(5)	1.14	1.08	1.14	1.08
5940 – 6210	$2\nu_2$, $\nu_1 + \nu_2$, $\nu_1 + \nu_3 + \nu_4$	0.79(5)	0.61	0.78	0.61	0.78
6210 – 6330	$2\nu_1$	0.48(5)	0.65	0.86	0.65	0.86

[a] Standard deviations in units of the last significant digits are given in parentheses.

[b] The values are the sum of the intensities computed for fundamental, overtone and combination bands comprised in the integration limits. HYB-MP2-1 refers to the model with CCSD(T)/CVTZ-ACTZ(F) harmonic intensities combined with anharmonic corrections computed at fc-MP2/CVTZ-ACVTZ(F) level, HYB-B2PLYP refers to the model with CCSD(T)/CVTZ-ACTZ(F) harmonic intensities combined with anharmonic corrections computed at B2PLYP/CVTZ-ACVTZ(F) level, HYB-MP2-2 refers to the model with fc-CCSD(T)/ANO2 harmonic intensities combined with anharmonic corrections computed at fc-MP2/CVTZ-ACVTZ(F) level, HYB-B2PLYP-2 refers to the model with fc-CCSD(T)/ANO2 harmonic intensities combined with anharmonic corrections computed at B2PLYP/CVTZ-ACVTZ(F) level.

Figure 1

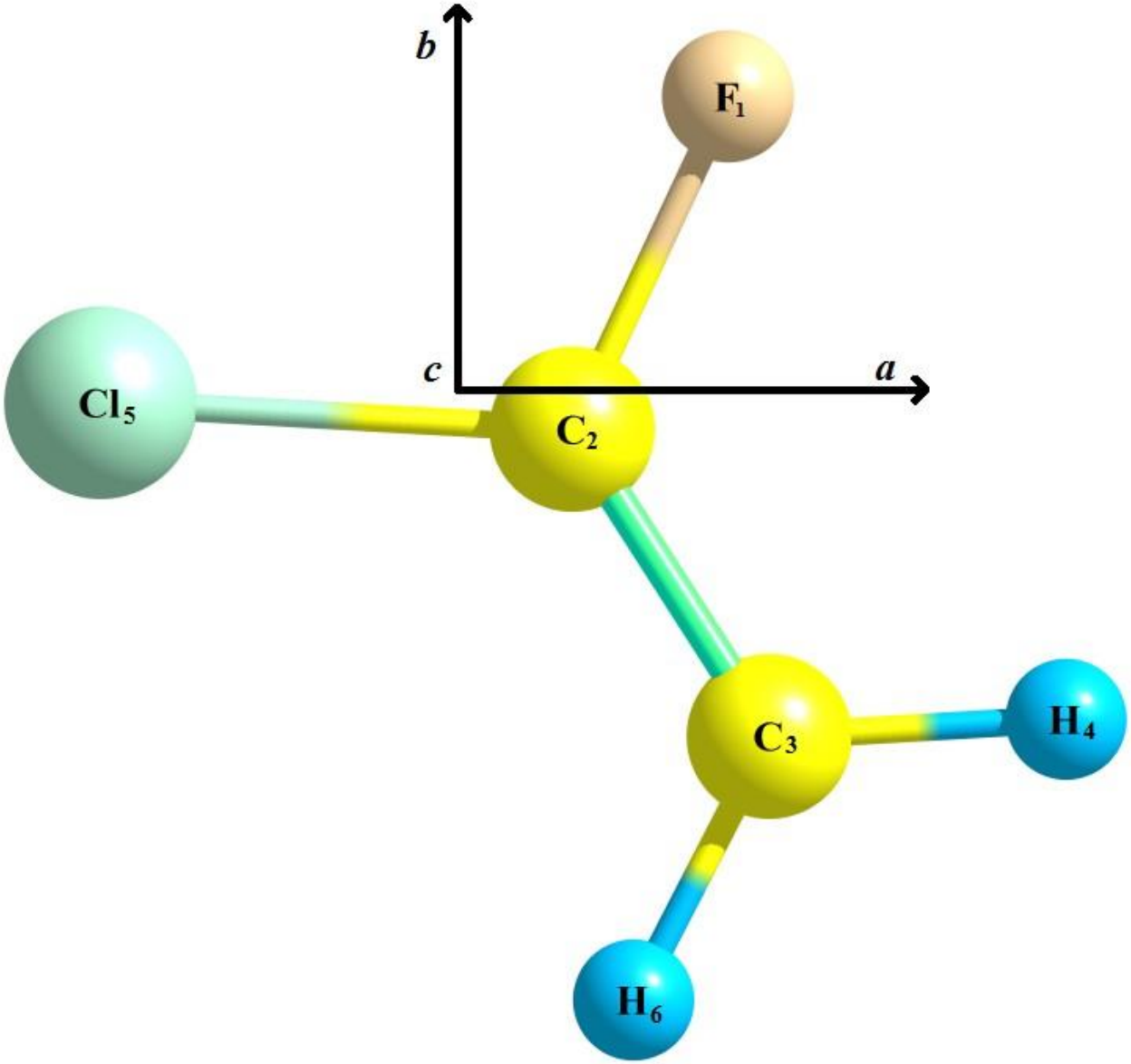

Figure 2

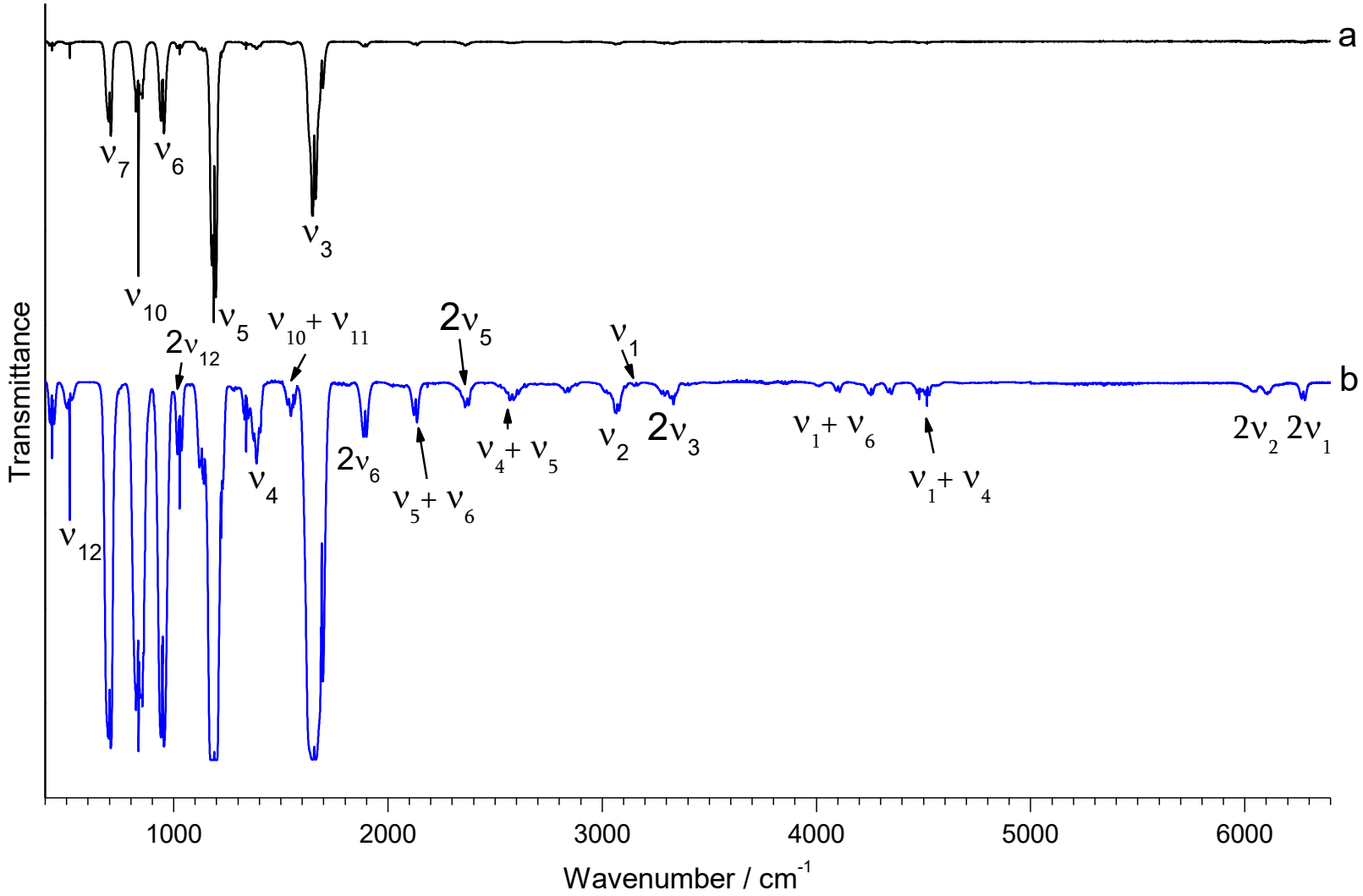
a
b
Transmittance
ν7
ν6
ν3
ν10
ν5
ν10+ ν11
2ν12
2ν5
ν1
ν12
ν4
2ν6
ν5+ ν6
ν4+ ν5
ν2
2ν3
ν1+ ν6
ν1+ ν4
2ν2 2ν1
1000
2000
3000
4000
5000
6000
Wavenumber / cm-1

Figure 3

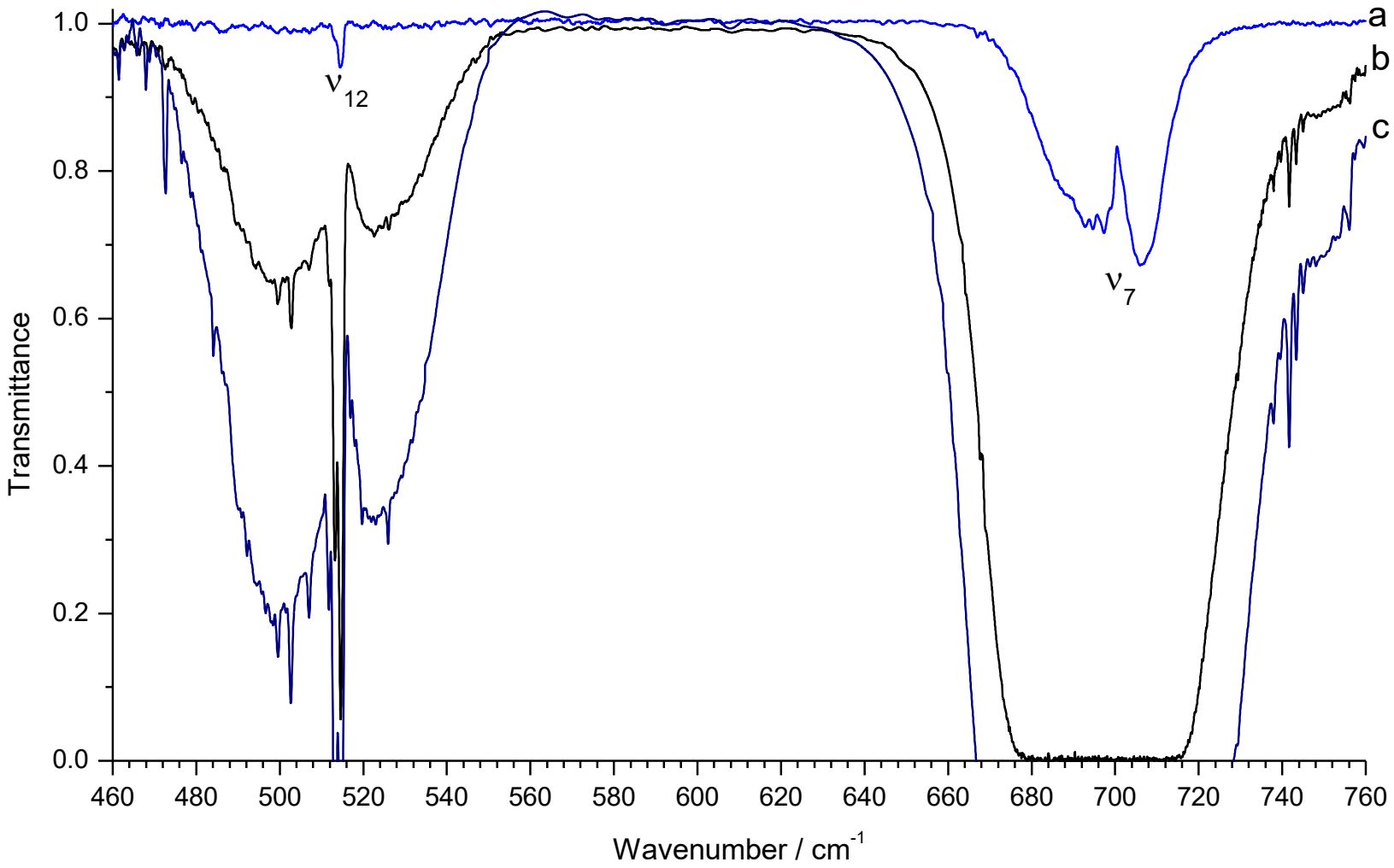
1.0
0.8
0.6
0.4
0.2
0.0
Transmittance
460
480
500
520
540
560
580
600
620
640
660
680
700
720
740
760
Wavenumber / cm-1
ν12
ν7
a
b
c

Figure 4

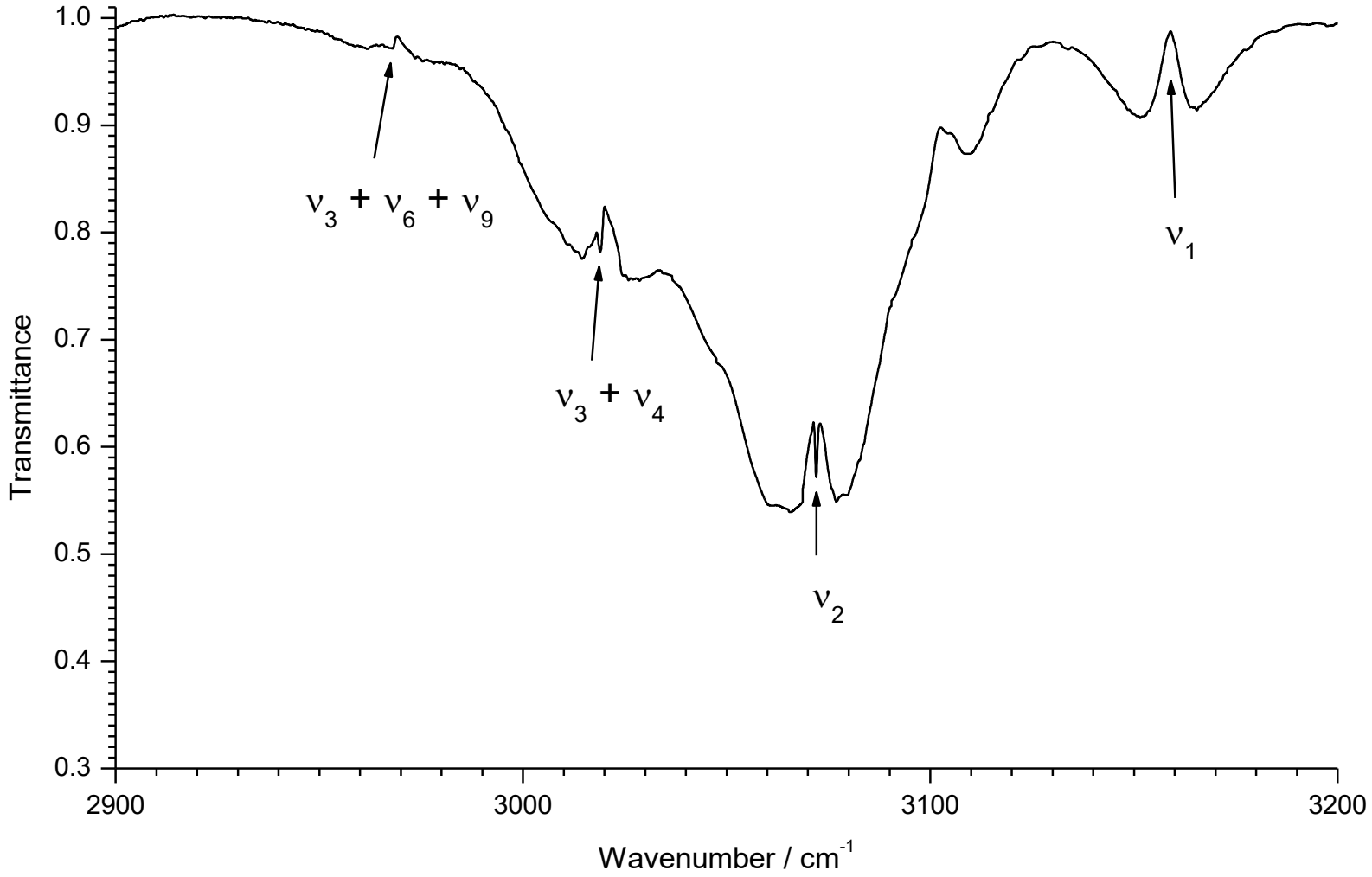
1.0
0.9
0.8
0.7
0.6
0.5
0.4
0.3
Transmittance
2900
3000
3100
3200
Wavenumber / cm-1
ν3 + ν6 + ν9
ν3 + ν4
ν2
ν1

Figure 5

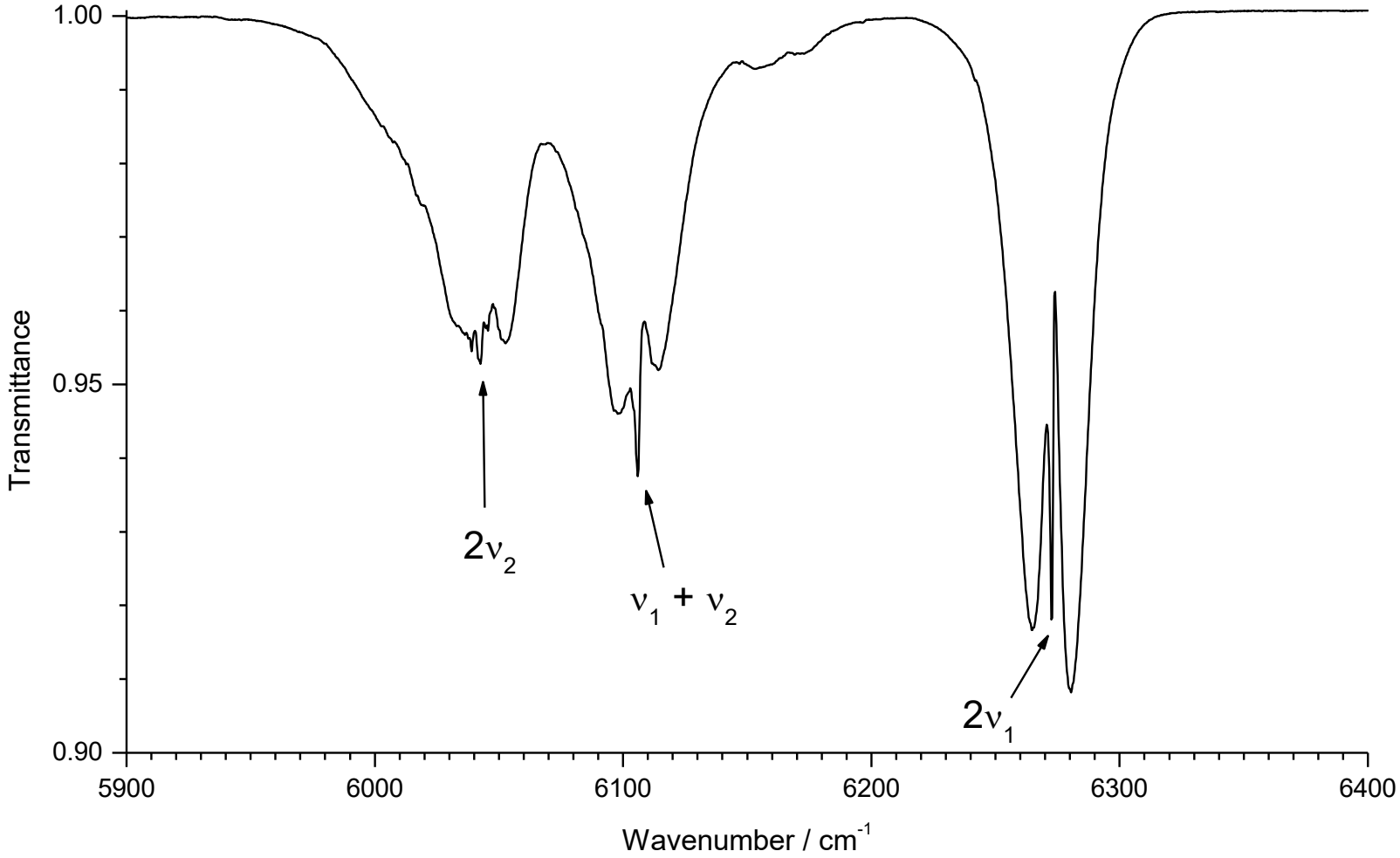
1.00
0.95
0.90
Transmittance
5900
6000
6100
6200
6300
6400
Wavenumber / cm-1
2ν2
ν1 + ν2
2ν1

Figure 6

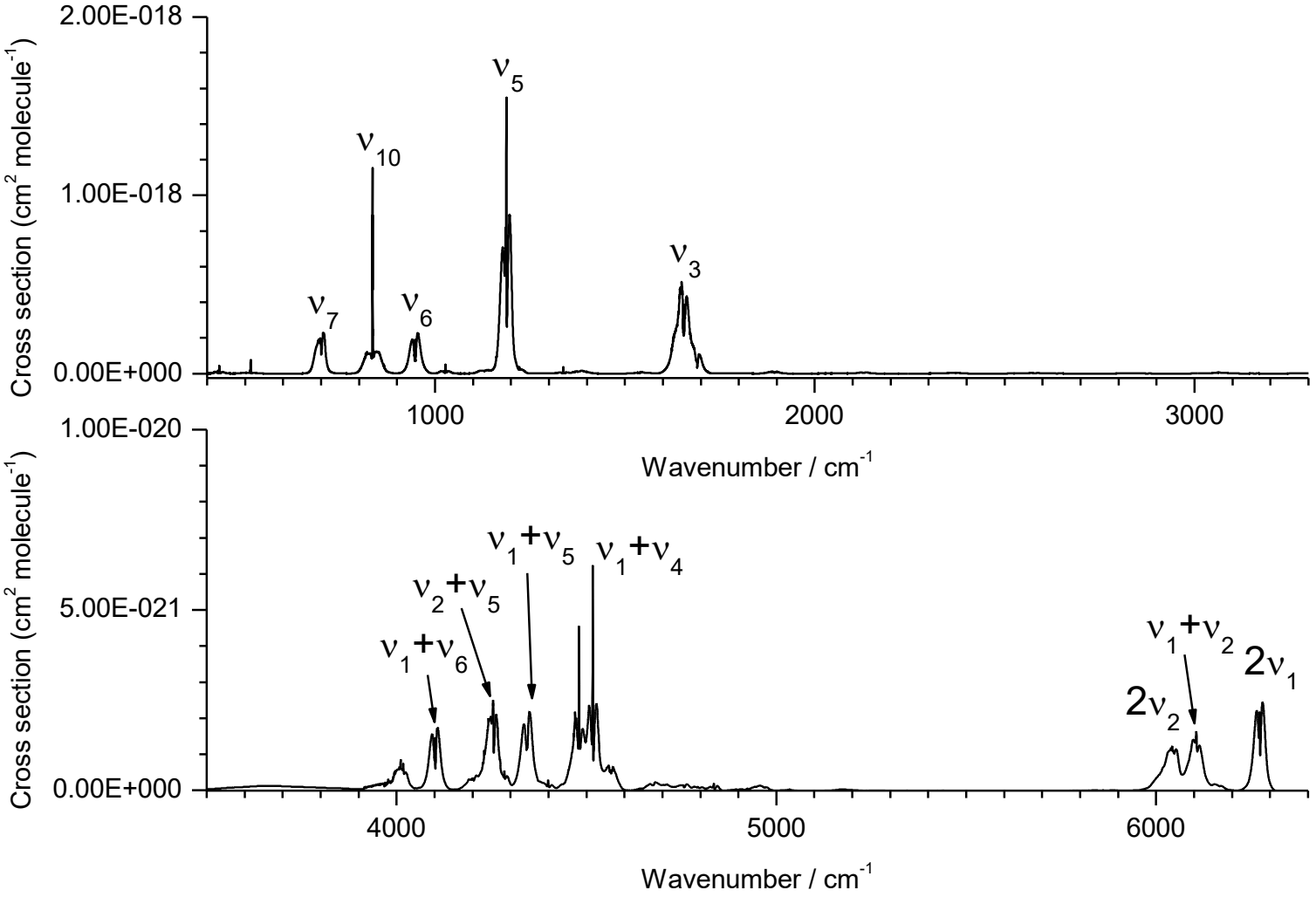
2.00E-018
1.00E-018
0.00E+000
Cross section (cm^2 molecule^{-1})
ν_5
ν_{10}
ν_3
ν_7
ν_6
1000
2000
3000
Wavenumber / cm^{-1}
1.00E-020
5.00E-021
0.00E+000
Cross section (cm^2 molecule^{-1})
$\nu_1+\nu_5$
$\nu_1+\nu_4$
$\nu_2+\nu_5$
$\nu_1+\nu_6$
$\nu_1+\nu_2$
$2\nu_1$
$2\nu_2$
4000
5000
6000
Wavenumber / cm^{-1}

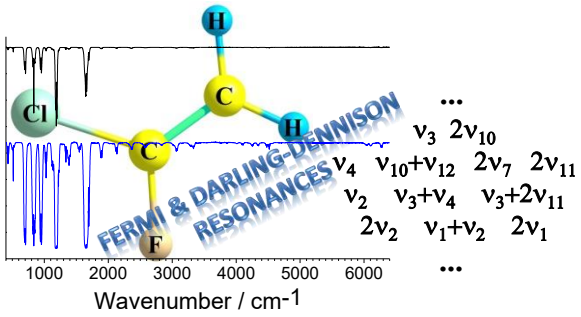
H
C
Cl
H
C
F
FERMI & DARLING-DENNISON RESONANCES
1000
2000
3000
4000
5000
6000
Wavenumber / cm-1
...
ν3 2ν10
ν4 ν10+ν12 2ν7 2ν11
ν2 ν3+ν4 ν3+2ν11
2ν2 ν1+ν2 2ν1
...